Shallow-water sloshing in vessels undergoing prescribed rigid-body motion in three dimensions

(draft version with colour figures)

HAMID ALEMI ARDAKANI AND THOMAS J. BRIDGES
Department of Mathematics, University of Surrey, Guildford, Surrey GU2 7XH England

(Received ?? and in revised form ??)

New shallow-water equations, for sloshing in three dimensions (two horizontal and one vertical) in a vessel which is undergoing rigid-body motion in 3−space, are derived. The rigid-body motion of the vessel (roll-pitch-yaw and/or surge-sway-heave) is modelled exactly and the only approximations are in the fluid motion. The flow is assumed to be inviscid but vortical, with approximations on the vertical velocity and acceleration at the surface. These equations improve previous shallow water models. The model also extends the essence of the Penney-Price-Taylor theory for the highest standing wave. The surface shallow water equations are simulated using an split-step implicit alternating direction finite-difference scheme. Numerical experiments are reported, including comparisons with existing results in the literature, and simulations with vessels undergoing full three-dimensional rotations.

1. Introduction

Shallow-water equations (SWEs) for a three-dimensional (3D) inviscid but vortical fluid in a vessel undergoing an arbitrary prescribed rigid-body motion in 3D are derived. The rigid body motion is represented exactly and only two assumptions are imposed on the velocity and acceleration at the free surface to close the SWEs.

While there has been a vast amount of research into two-dimensional sloshing, the research into 3D sloshing is still very much in development. A review of much of the research to date is presented in Ibrahim (2005). The predominant theoretical approaches for studying 3D sloshing are (a) asymptotics and weakly nonlinear theories, (b) multi-modal expansions which reduce the governing equations to a set of ordinary differential equations; (c) reduction to model partial differential equations such as the shallow water equations; and (d) direct numerical simulation of the full 3D problem.

If 3D numerical simulations were faster, the latter approach would be very appealing. There has been much progress in the numerical simulation of 3D sloshing using Navier-Stokes based methods (MAC, SURF, VOF, RANSE), boundary-element methods and finite-element methods for 3D potential flow (some examples are Lee *et al.* 2007; Kim 2001; Liu & Lin 2008; Buchner 2002; Kleefsman *et al.* 2005; Gerrits 2001; aus der Wiesche 2003; Chen *et al.* 2009; Cariou & Casella 1999; Chen *et al.* 2000; Wu *et al.* 1998). While the results of these simulations are impressive, the difficulty is that CPU times are measured in hours rather than seconds or minutes. An example is the VOF simulations of Liu & Lin (2008), where 3D sloshing in a vessel with rectangular base is forced harmonically. To simulate 50 seconds of real time (about 20 periods of harmonic forcing) took 265 hours of CPU time. It is very difficult to do parametric studies or long time simulations with this amount of CPU time. Hence any reduction in dimension is appealing.

On the other hand one can make some progress in the understanding of sloshing in 3D using analytical methods, asymptotics (perturbation theory, multi-scale expansions) and modal expansions. In 2D shallow water sloshing the predominant types of solution are the standing wave and travelling hydraulic jump. But in 3D shallow water sloshing the range of basic solutions is much larger. One still has the 2D solutions, but there can be mixed modes, swirling modes, multi-mode cnoidal standing waves and multi-dimensional hydraulic jumps and analytical methods are very effective for identifying parameter regimes for these basic solutions (e.g. Faltinsen *et al.* 2003, 2006*a*; Faltinsen & Timokha

2003; Bridges 1987). And, there is a vast literature on asymptotic methods for the special case of parametrically-forced sloshing in rectangular containers (Faraday experiment) (e.g. Miles & Henderson 1990, and its citation trail). Multi-modal expansions take analytic methods to higher order. When the fluid domain is finite in extent there is a countable basis of eigenfunctions for the basin shape, and one approach that has been extensively used is to expand the nonlinear equations in terms of these (or other) basis functions with time-dependent coefficients, leading to a large system of ordinary differential equations. Examples of this approach are Faltinsen & Timokha (2003); Faltinsen *et al.* (2003, 2006*a*); La Rocca *et al.* (1997, 2000) and (Part II of Ibrahim 2005). The advantage of modal approximation is that the problem is reduced to a system of ODEs which is much quicker to simulate numerically.

In between direct 3D simulations and analytical methods is a third approach: to derive reduced PDE models. This approach is particularly useful for the study of shallow water sloshing. The study of 3D shallow-water sloshing is motivated by a number of applications such as: sloshing on the deck of fishing vessels (Caglayan & Storch 1982; Adee & Caglayan 1982) and offshore suppy vessels (Falzarano *et al.* 2002), sloshing in wing fuel tanks of aircraft (Disimile *et al.* 2009), green-water effects (Dillingham & Falzarano 1986; Zhou *et al.* 1999; Buchner 2002; Kleefsman *et al.* 2005), sloshing in a swimming pool on deck (Ruponen *et al.* 2009), sloshing in fish tanks onboard fishing vessels (Lee *et al.* 2005), and sloshing in automobile fuel tanks (aus der Wiesche 2003).

About the same time, Dillingham & Falzarano (1986) and Pantazopoulos (1987) (see also Pantazopoulos & Adee (1987) and Pantazopoulos (1988)) derived shallow water equations for 3D sloshing with the vessel motion prescribed. It is this approach that is the starting point for the current paper. These SWEs, hereafter called the DFP SWEs, will be recorded and analyzed in §9. In followup work Huang (1995) (see also Huang & Hsiung (1996) and Huang & Hsiung (1997)) gave an alternative derivation of rotating SWEs for sloshing resulting in slightly different equations from the DFP SWEs. The latter system will be called the HH SWEs. A discussion of the HH SWEs is also given in §9.

The DFP SWEs use a very simple form for the vessel motion, and have unecessarily restrictive assumptions in the derivation. The derivation of the HH SWEs is more precise but still has some restrictive assumptions. These assumptions are outlined in §9 and in more detail in the technical reports of Alemi Ardakani & Bridges (2009*d*,*e*).

In this paper a new derivation of SWEs in 3D is given which leads to exact SWEs for the horizontal velocity field at the free surface of the form

$$\begin{aligned} U_t + UU_x + VU_y + \left(a_{11} + \tfrac{Dw}{Dt}\big|^h\right) h_x + a_{12}h_y &= b_1 + \sigma\partial_x \mathsf{div}(\boldsymbol{\kappa}) \\ V_t + UV_x + VV_y + \left(a_{22} + \tfrac{Dw}{Dt}\big|^h\right) h_y + a_{21}h_x &= b_2 + \sigma\partial_y \mathsf{div}(\boldsymbol{\kappa})\,. \end{aligned} \tag{1.1}$$

These equations are relative to a frame of reference moving with the vessel with coordinates (x, y, z) and z vertical. The terms $a_{11}, a_{12}, a_{21}, a_{22}, b_1, b_2$ encode the moving frame, κ is a curvature term associated with surface tension, and $\frac{Dw}{Dt}\big|^h$ is the Lagrangian vertical acceleration at the free surface. The fluid occupies a rectangular region with a single-valued free surface,

$$0 \leqslant z \leqslant h(x, y, t)\,, \quad 0 \leqslant x \leqslant L_1\,, \quad 0 \leqslant y \leqslant L_2\,.$$

The free surface horizontal velocity field is

$$U(x, y, t) = u(x, y, z, t)\big|^h := u(x, y, h(x, y, t), t) \quad \text{and} \quad V(x, y, t) = v(x, y, z, t)\big|^h\,.$$

Couple the equations (1.1) with the exact mass conservation equation

$$h_t + (hU)_x + (hV)_x = W + hU_x + hV_y\,, \tag{1.2}$$

which is derived from the kinematic free surface boundary condition (see §2). $W = w\big|^h$ is the vertical velocity at the free surface.

By assuming that $\frac{Dw}{Dt}\big|^h \approx 0$ and $W + hU_x + hV_y \approx 0$ the equations (1.1)-(1.2) are a closed set of SWEs which retain the vessel motion exactly. It is this closed set of SWEs that is the starting point for the analysis and numerics in this paper.

One of the advantages of the SWEs is that vorticity is retained. This is in contrast to almost all analytical research into 3D sloshing which uses the assumption of irrotationality. Vorticity can be input through the initial conditions, but a new mechanism comes into play in shallow water sloshing: the creation of vorticity though discontinuities in hydraulic jumps (e.g. Peregrine 1998, 1999). In coastal hydraulics Peregrine (1998) has shown how steady hydraulic jumps generate vorticity. In the case of shallow water sloshing there is a dynamic mechanism due to the time-dependent nature of the hydraulic jumps, and this phenomena is witnessed in some of the numerical simulations reported herein.

In special cases the surface SWEs (1.1)-(1.2) have a form of potential vorticity (PV) conservation. For example when the vessel is undergoing pure yaw motion, then a form of PV is conserved. This PV is different from that appearing in geophysical fluid dynamics. In geophysical fluid dynamics the rotation (rotation of the earth) is treated as a constant, whereas here the rotation is time dependent. On the other hand, Barnes *et al.* (1983) have shown that the earth does indeed wobble and so the idea of time-dependent yaw motion has some relation to geophysical fluid dynamics.

The vessel is modelled as a rigid body, and the position of a rigid body in 3−space is completely determined by specifying $(\mathbf{q}(t), \mathbf{Q}(t))$ where $\mathbf{q}(t)$ is a vector in $\mathbb{R}^3$ giving the horizontal and vertical translation of the body relative to some fixed reference frame, and $\mathbf{Q}$ is a proper 3×3 rotation matrix ($\mathbf{Q}$ is orthogonal and $\det(\mathbf{Q}) = 1$).

Specifying translations is straightfoward, but specifying rotations requires a little more care. Surprisingly most previous work on forced sloshing uses pure translation, or the rotations are simplified using a small angle approximation or restricted to planar rotations. The small angle approximation is to take the angular velocity of the form $\mathbf{\Omega} = (\dot{\phi}, \dot{\theta}, \dot{\psi})$ where ϕ, θ and ψ are roll, pitch and yaw angles respectively (precise definition given in §8.2). Examples of forcing used in the literature are Chen *et al.* (2009) (harmonic surge and sway motion, and harmonic roll motion); Wu *et al.* (1998) (harmonic surge, sway and heave forcing); Chen *et al.* (2000) and Faltinsen *et al.* (2006*a*) (harmonic surge forcing); aus der Wiesche (2003) (impulse excitation representative of automobile accelerations); Faltinsen *et al.* (2006*b*) (roll-pitch forcing with a small angle approximation); Liu & Lin (2008) and Wu & Chen (2009) include forcing in all 6 degrees of freedom, but the rotations use the small angle approximation.

In this paper exact representations of the rotations are used. Both Euler angle representations and numerical construction of the rotation matrix are used. The choice (body or space) representation of the angular velocity is important and its implications are discussed. Also their are subtleties in the construction of the angular velocity (Leubner 1981) and these are also discussed herein and in the report of Alemi Ardakani & Bridges (2009*f*).

There has been very little experimental work with vessels undergoing full 3D rotations. Most experiments are with pure translations and/or planar rotations. A facility for 3D rotations of vessels with fluid would be technically demanding. However, the paper of Disimile *et al.* (2009) mentions an experimental facility capable of exciting a tank containing fluid in all 6 degrees of freedom. However, to date they have only reported on results of forced roll motion.

Our principal tool for analyzing the SWEs is numerics. The numerical scheme is based on the Abbott-Ionescu scheme which is widely used in computational hydraulics. It is a finite-difference scheme, fully implicit, and the two-dimensionality is treated using an alternating direction implicit scheme. A one-dimensional version of this scheme was used in Alemi Ardakani & Bridges (2009*g*).

An overview of the paper is as follows. In §§3-4 the SWEs (1.1) for sloshing in a vessel undergoing motion in 3-space are derived starting from the full 3D Euler equations relative to a moving frame.

Before assuming that the Lagrangian vertical accelerations are small we analyze the exact equations in §5 and show that they give an explanation for and a generalization to 3D of the Penney-Price-Taylor theory for the highest standing wave.

The assumptions necessary for the reduction to a closed set of SWEs with the body motion exact are discussed in §7, leading to a closed set of SWEs.

Details of the specification of the vessel motion are given in §8, including both an Euler angle representation and direction calculation of the rotation matrix numerically. Further detail on the special case of yaw-pitch-roll Euler angles is given in the report of Alemi Ardakani & Bridges (2009*c*).

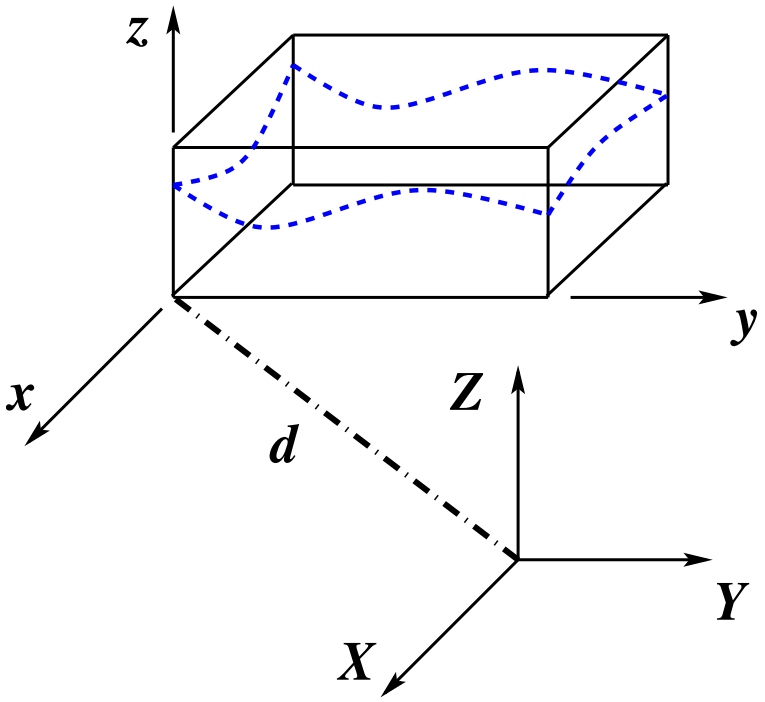

FIGURE 1. Schematic showing a configuration of the fixed coordinate system $OXYZ$ relative to the moving coordinate system, attached to the tank, $Oxyz$. The origin of the OXYZ coordinate system can have an additional displacement $\mathbf{q}(t)$. In this figure $\mathbf{q}(t) = 0$.

The DFP SWEs and HH SWEs are reviewed in the reports of Alemi Ardakani & Bridges (2009*d*) and Alemi Ardakani & Bridges (2009*e*). A summary of the main assumptions in their derivation and a comparison with the new surface SWEs is given in §9.

The numerical algorithm is introduced in §10. Further detail on the numerical scheme is contained in the technical report of Alemi Ardakani & Bridges (2009*f*).

Numerical results are reported in Sections 11 to 14. These simulations include full 3D rotations: roll-pitch in §11 and yaw-pitch-roll in §14. Results of pure yaw forcing are report in §12. These simulations show the appearance of vorticity, agree with previous simulations of Huang & Hsiung (1996) and conserve a time-dependent form of potential vorticity. Motivated by simulations of Wu & Chen (2009), diagonal surge-sway forcing is considered in §13, illustrating planarization of waves and the appearance of square-like waves.

2. Governing equations

The configuration of the fluid in a rotating-translating vessel is shown schematically in Figure 1. The vessel is a rigid body which is free to rotate and or translate in $\mathbb{R}^3$, and this motion will be specified. The spatial frame, which is fixed in space, has coordinates denoted by $\mathbf{X} = (X, Y, Z)$, and the body frame – a moving frame – is attached to the vessel and has coordinates denoted by $\mathbf{x} = (x, y, z)$.

The whole system is translating in space with translation vector $\mathbf{q}(t)$. The position of a particle in the body frame is therefore related to a point in the spatial frame by

$$\mathbf{X} = \mathbf{Q}(\mathbf{x} + \mathbf{d}) + \mathbf{q}\,,$$

where $\mathbf{Q}$ is a proper rotation in $\mathbb{R}^3$ ($\mathbf{Q}^T = \mathbf{Q}^{-1}$ and $\det(\mathbf{Q}) = 1$). The axis of rotation can be displaced a distance $\mathbf{d}$ from the origin of the body frame and $\mathbf{d} = (d_1, d_2, d_3) \in \mathbb{R}^3$ is constant. The displacement $\mathbf{Qd}$ could be incorporated into $\mathbf{q}(t)$ but in cases where the origin of the spatial frame is fixed, it will be useful to maintain the distinction.

This formulation is consistent with the theory of rigid body motion, where an arbitrary motion

can be described by the pair $(\mathbf{Q}(t), \mathbf{q}(t))$ with $\mathbf{Q}(t)$ a proper rotation matrix and $\mathbf{q}(t)$ a vector in $\mathbb{R}^3$ (O'Reilly 2008; Murray *et al.* 1994).

The *body angular velocity* is a time-dependent vector

$$\mathbf{\Omega}(t) = (\Omega_1(t), \Omega_2(t), \Omega_3(t))\,,$$

with entries determined from $\mathbf{Q}$ by

$$\mathbf{Q}^T\dot{\mathbf{Q}} = \begin{bmatrix} 0 & -\Omega_3 & \Omega_2 \\ \Omega_3 & 0 & -\Omega_1 \\ -\Omega_2 & \Omega_1 & 0 \end{bmatrix} := \widehat{\mathbf{\Omega}}\,. \tag{2.1}$$

The convention for the entries of the skew-symmetric matrix $\widehat{\Omega}$ is such that

$$\widehat{\mathbf{\Omega}}\mathbf{r} = \mathbf{\Omega} \times \mathbf{r}\,, \quad \text{for any} \quad \mathbf{r} \in \mathbb{R}^3\,, \quad \mathbf{\Omega} := (\Omega_1, \Omega_2, \Omega_3)\,.$$

The body angular velocity is to be contrasted with the *spatial angular velocity* – the angular velocity viewed from the spatial frame – which is

$$\widehat{\mathbf{\Omega}}^{\text{spatial}} := \dot{\mathbf{Q}}\mathbf{Q}^T\,.$$

As vectors the spatial and body angular velocities are related by $\mathbf{\Omega}^{\text{spatial}} = \mathbf{Q}\mathbf{\Omega}$. Either representation for the angular velocity can be used. For example Pantazopoulos (1988); Dillingham & Falzarano (1986); Falzarano *et al.* (2002); Pantazopoulos & Adee (1987) all use the spatial representation, whereas Huang & Hsiung (1996, 1997) use the body representation. We will show that the body representation is the sensible choice leading to great simplification of the equations. Henceforth, the angular velocity without a superannotation will represent the body angular velocity.

The velocity and acceleration in the spatial frame are

$$\dot{\mathbf{X}} = \mathbf{Q}(\dot{\mathbf{x}} + \mathbf{\Omega} \times (\mathbf{x} + \mathbf{d})) + \dot{\mathbf{q}}\,. \tag{2.2}$$

and

$$\ddot{\mathbf{X}} = \mathbf{Q}[\ddot{\mathbf{x}} + 2\mathbf{\Omega} \times \dot{\mathbf{x}} + \dot{\mathbf{\Omega}} \times (\mathbf{x} + \mathbf{d}) + \mathbf{\Omega} \times \mathbf{\Omega} \times (\mathbf{x} + \mathbf{d}) + \mathbf{Q}^T\ddot{\mathbf{q}}]\,. \tag{2.3}$$

Newton's law is expressed relative to the spatial frame, but substitution of (2.2)-(2.3) into Newton's law and multiplying by $\mathbf{Q}^T$ gives the governing equations relative to the body frame,

$$\frac{D\mathbf{u}}{Dt} + \frac{1}{\rho}\nabla p + 2\mathbf{\Omega} \times \mathbf{u} + \dot{\mathbf{\Omega}} \times (\mathbf{x} + \mathbf{d}) + \mathbf{\Omega} \times (\mathbf{\Omega} \times (\mathbf{x} + \mathbf{d})) + \mathbf{Q}^T\mathbf{g} + \mathbf{Q}^T\ddot{\mathbf{q}} = 0\,, \tag{2.4}$$

where $\mathbf{u} = (u, v, w)$ is the velocity field,

$$\frac{D}{Dt} := \frac{\partial}{\partial t} + u\frac{\partial}{\partial x} + v\frac{\partial}{\partial y} + w\frac{\partial}{\partial z} \quad \text{and} \quad \mathbf{g} := g\begin{pmatrix} 0 \\ 0 \\ 1 \end{pmatrix}\,,$$

with $g > 0$ the gravitational constant. A detailed derivation is given in Appendix A of Alemi Ardakani & Bridges (2009*g*). The term $\mathbf{Q}^T\mathbf{g}$ rotates the usual gravity vector so that its direction is properly viewed in the body frame. Similarly for the translational acceleration $\ddot{\mathbf{q}}$. Further comments on the viewpoint of the vessel velocity and acceleration are in §8.

In the derivation of the SWEs the components of (2.4) will be needed. Write the momentum equation as

$$\frac{D\mathbf{u}}{Dt} + \frac{1}{\rho}\nabla p = \mathbf{F}\,, \tag{2.5}$$

then

$$\mathbf{F} = -2\mathbf{\Omega} \times \mathbf{u} - \dot{\mathbf{\Omega}} \times (\mathbf{x} + \mathbf{d}) - \mathbf{\Omega} \times (\mathbf{\Omega} \times (\mathbf{x} + \mathbf{d})) - \mathbf{Q}^T\mathbf{g} - \mathbf{Q}^T\ddot{\mathbf{q}}\,,$$

and the components of $\mathbf{F}$ are

$$\begin{aligned}
F_1 &= -2(\Omega_2 w - \Omega_3 v) - \dot{\Omega}_2(z+d_3) + \dot{\Omega}_3(y+d_2) \\
&\quad -\Omega_1\,\boldsymbol{\Omega}\cdot(\mathbf{x}+\mathbf{d}) + (x+d_1)\|\boldsymbol{\Omega}\|^2 - \ddot{\mathbf{q}}\cdot\mathbf{Q}\mathbf{e}_1 - g\mathbf{e}_3\cdot\mathbf{Q}\mathbf{e}_1 \\
F_2 &= +2(\Omega_1 w - \Omega_3 u) + \dot{\Omega}_1(z+d_3) - \dot{\Omega}_3(x+d_1) \\
&\quad -\Omega_2\,\boldsymbol{\Omega}\cdot(\mathbf{x}+\mathbf{d}) + (y+d_2)\|\boldsymbol{\Omega}\|^2 - \ddot{\mathbf{q}}\cdot\mathbf{Q}\mathbf{e}_2 - g\mathbf{e}_3\cdot\mathbf{Q}\mathbf{e}_2 \\
F_3 &= -2(\Omega_1 v - \Omega_2 u) - \dot{\Omega}_1(y+d_2) + \dot{\Omega}_2(x+d_1) \\
&\quad -\Omega_3\,\boldsymbol{\Omega}\cdot(\mathbf{x}+\mathbf{d}) + (z+d_3)\|\boldsymbol{\Omega}\|^2 - \ddot{\mathbf{q}}\cdot\mathbf{Q}\mathbf{e}_3 - g\mathbf{e}_3\cdot\mathbf{Q}\mathbf{e}_3\,.
\end{aligned}$$

The fluid occupies the region

$$0 \leqslant x \leqslant L_1\,, \quad 0 \leqslant y \leqslant L_2\,, \quad 0 \leqslant z \leqslant h(x,y,t)\,,$$

where the lengths L_1 and L_2 are given positive constants, and $z = h(x,y,t)$ is the position of the free surface.

Conservation of mass relative to the body frame takes the usual form

$$u_x + v_y + w_z = 0\,. \tag{2.6}$$

The boundary conditions are

$$\begin{aligned}
u = 0 \quad \text{at} \quad x = 0 \quad \text{and} \quad x = L_1 \\
v = 0 \quad \text{at} \quad y = 0 \quad \text{and} \quad y = L_2 \\
w = 0 \quad \text{at} \quad z = 0\,,
\end{aligned} \tag{2.7}$$

and at the free surface the boundary conditions are the kinematic condition

$$h_t + uh_x + vh_y = w\,, \quad \text{at} \quad y = h(x,t)\,, \tag{2.8}$$

and the dynamic condition

$$p = -\rho\sigma\,\mathsf{div}(\boldsymbol{\kappa}) \quad \text{at} \quad y = h(x,t)\,, \tag{2.9}$$

where $\sigma > 0$ is the coefficient of surface tension,

$$\mathsf{div}(\boldsymbol{\kappa}) = \frac{\partial \kappa_1}{\partial x} + \frac{\partial \kappa_2}{\partial y}\,,$$

and

$$\kappa_1 = \frac{h_x}{\sqrt{1+h_x^2+h_y^2}} \quad \text{and} \quad \kappa_1 = \frac{h_y}{\sqrt{1+h_x^2+h_y^2}}\,.$$

2.1. *Vorticity*

The vorticity vector is defined by

$$\mathcal{V} := \nabla \times \mathbf{u}\,,$$

Differentiating this equation gives

$$\frac{D\mathcal{V}}{Dt} = \mathcal{V}\cdot\nabla\mathbf{u} + \nabla\times\left(\frac{D\mathbf{u}}{Dt}\right)\,. \tag{2.10}$$

Taking the curl of the momentum equations (2.4) gives

$$\nabla\times\left(\frac{D\mathbf{u}}{Dt}\right) = 2\boldsymbol{\Omega}\cdot\nabla\mathbf{u} - 2\dot{\boldsymbol{\Omega}}\,.$$

Combining with (2.10) gives the vorticity equation

$$\frac{D\mathcal{V}}{Dt} = (2\boldsymbol{\Omega} + \mathcal{V})\cdot\nabla\mathbf{u} - 2\dot{\boldsymbol{\Omega}}\,.$$

Two components of the vorticity equation will be important in the derivation of the surface SWEs,

$$\begin{aligned}\frac{\partial}{\partial y}\left(\frac{Dw}{Dt}\right) &= \frac{\partial}{\partial z}\left(\frac{Dv}{Dt}\right) + 2\Omega_1\frac{\partial u}{\partial x} + 2\Omega_2\frac{\partial u}{\partial y} + 2\Omega_3\frac{\partial u}{\partial z} - 2\dot\Omega_1\\ \frac{\partial}{\partial x}\left(\frac{Dw}{Dt}\right) &= \frac{\partial}{\partial z}\left(\frac{Dv}{Dt}\right) - 2\Omega_1\frac{\partial v}{\partial x} - 2\Omega_2\frac{\partial v}{\partial y} - 2\Omega_3\frac{\partial v}{\partial z} + 2\dot\Omega_2\,.\end{aligned} \tag{2.11}$$

3. Reduction of the pressure gradient

The derivation of the SWEs in 3D (1.1) follows the same strategy as the 2D case in Alemi Ardakani & Bridges (2009*g*). The key is the precise treatment of the pressure field. Let

$$\beta(x,y,t) = -\dot\Omega_1(y+d_2) + \dot\Omega_2(x+d_1) - \Omega_3\Omega_1(x+d_1) - \Omega_3\Omega_2(y+d_2) - \mathbf{Q}\mathbf{e}_3\cdot\ddot{\mathbf{q}} - g\mathbf{Q}\mathbf{e}_3\cdot\mathbf{e}_3\,. \tag{3.1}$$

Then the vertical momentum equation can be expressed in the form

$$\frac{Dw}{Dt} + \frac{1}{\rho}\frac{\partial p}{\partial z} = -2(\Omega_1 v - \Omega_2 u) + (\Omega_1^2+\Omega_2^2)(z+d_3) + \beta(x,y,t)\,.$$

Integrate from z to h,

$$\begin{aligned}\int_z^h \frac{Dw}{Dt}\,\mathrm{d}s + \frac{1}{\rho}p\Big|_z^h &= -2\Omega_1\int_z^h v\,\mathrm{d}s + 2\Omega_2\int_z^h u\,\mathrm{d}s\\ &\quad +(\Omega_1^2+\Omega_2^2)(\tfrac12 h^2 - \tfrac12 z^2 + d_3h - d_3z) + \beta(x,y,t)(h-z)\,.\end{aligned}$$

Applying the surface boundary condition on the pressure then gives the pressure at any point z,

$$\begin{aligned}\frac{1}{\rho}p(x,y,z,t) &= \int_z^h \frac{Dw}{Dt}\,\mathrm{d}s + 2\Omega_1\int_z^h v\,\mathrm{d}s - 2\Omega_2\int_z^h u\,\mathrm{d}s - \beta(x,y,t)(h-z)\\ &\quad -(\Omega_1^2+\Omega_2^2)(\tfrac12 h^2 - \tfrac12 z^2 + d_3h - d_3z) - \sigma\mathsf{div}(\boldsymbol{\kappa})\,.\end{aligned} \tag{3.2}$$

This equation for $p(x,y,z,t)$ is exact. The strategy is to take derivatives with respect to x and y and then substitute into the horizontal momentum equations. The details are lengthy and are given in Appendix A. The expressions are

$$\begin{aligned}\frac{1}{\rho}\frac{\partial p}{\partial x} &= \frac{Du}{Dt}\Big|_z^h + \frac{Dw}{Dt}\Big|^h h_x + 2\Omega_2 W - 2\Omega_3 V + 2\dot\Omega_2(h-z) - 2\Omega_2 w + 2\Omega_3 v\\ &\quad +2\Omega_1 V h_x - 2\Omega_2 U h_x - (\Omega_1^2+\Omega_2^2)(h+d_3)h_x - \beta_x(h-z) - \beta h_x - \sigma\partial_x\,\mathsf{div}(\boldsymbol{\kappa})\,.\end{aligned} \tag{3.3}$$

and

$$\begin{aligned}\frac{1}{\rho}\frac{\partial p}{\partial y} &= \frac{Dv}{Dt}\Big|_z^h + \frac{Dw}{Dt}\Big|^h h_y - 2\Omega_1 W + 2\Omega_3 U - 2\dot\Omega_1(h-z) + 2\Omega_1 w - 2\Omega_3 u\\ &\quad +2\Omega_1 V h_y - 2\Omega_2 U h_y - (\Omega_1^2+\Omega_2^2)(h+d_3)h_y - \beta_y(h-z) - \beta h_y - \sigma\partial_y\,\mathsf{div}(\boldsymbol{\kappa})\,.\end{aligned} \tag{3.4}$$

The pressure is eliminated from the horizontal momentum equations using (3.3) and (3.4). The details will be given for the $x-$momentum equation and then the result will be stated for the $y-$momentum equation.

4. Reduction of the horizontal momentum equation

The $x-$component of the momentum equations (2.4) is

$$\begin{aligned}\frac{Du}{Dt} + \frac{1}{\rho}\frac{\partial p}{\partial x} &= -2(\Omega_2 w - \Omega_3 v) - \dot\Omega_2(z+d_3) + \dot\Omega_3(y+d_2)\\ &\quad -\Omega_1\,\boldsymbol{\Omega}\cdot(\mathbf{x}+\mathbf{d}) + (x+d_1)\|\boldsymbol{\Omega}\|^2 - \mathbf{Q}\mathbf{e}_1\cdot\ddot{\mathbf{q}} - g\mathbf{Q}\mathbf{e}_1\cdot\mathbf{e}_3\,.\end{aligned} \tag{4.1}$$

Replace the second term on the left-hand side by the expression for $\rho^{-1}p_x$ in (3.3),

$$\begin{aligned}\frac{Du}{Dt}+\frac{Du}{Dt}\Big|_z^h+\frac{Dw}{Dt}\Big|^h h_x &= -2\Omega_2 W+2\Omega_3 V-2\dot\Omega_2(h-z)\\ &\quad -2\Omega_1 V h_x+2\Omega_2 U h_x+2\Omega_2 w-2\Omega_3 v\\ &\quad +(\Omega_1^2+\Omega_2^2)(h+d_3)h_x+\beta_x(h-z)+\beta h_x+\sigma\partial_x\mathsf{div}(\boldsymbol{\kappa})\\ &\quad -2(\Omega_2 w+\Omega_3 v)-\dot\Omega_2(z+d_3)+\dot\Omega_3(y+d_2)\\ &\quad -\Omega_1\,\boldsymbol{\Omega}\cdot(\mathbf{x}+\mathbf{d})+(x+d_1)\|\boldsymbol{\Omega}\|^2-\mathbf{Q}\mathbf{e}_1\cdot\ddot{\mathbf{q}}-g\mathbf{Q}\mathbf{e}_1\cdot\mathbf{e}_3\,.\end{aligned}$$

There are convenient cancellations: principally $\frac{Du}{Dt}$, $2\dot\Omega z$ and the interior Coriolis terms all cancel out. Cancelling and using $\beta_x=\dot\Omega_2-\Omega_1\Omega_3$, and the kinematic condition $W=h_t+Uh_x+Vh_y$ gives

$$\begin{aligned}&\tfrac{Du}{Dt}\Big|^h+\tfrac{Dw}{Dt}\Big|^h h_x+2\Omega_2(h_t+Uh_x+Vh_y)-2\Omega_3 V+2\Omega_1 V h_x-2\Omega_2 U h_x\\ &-(\Omega_1^2+\Omega_2^2)(h+d_3)h_x-(\Omega_2^2+\Omega_3^2)(x+d_1)+\Omega_1\Omega_2(y+d_2)+\Omega_1\Omega_3(h+d_3)\\ &+\dot\Omega_2(h+d_3)-\dot\Omega_3(y+d_2)+\mathbf{Q}\mathbf{e}_1\cdot\ddot{\mathbf{q}}+g\mathbf{Q}\mathbf{e}_1\cdot\mathbf{e}_3-\beta h_x-\sigma\partial_x\mathsf{div}(\boldsymbol{\kappa})=0\,.\end{aligned}\tag{4.2}$$

Now use the fact that $\frac{Du}{Dt}\Big|^h$ can be expressed purely in terms of surface variables since,

$$U_t+UU_x+VU_y=\frac{Du}{Dt}\Big|^h\,.$$

Substition into (4.2) reduces the $x-$momentum equation to an equation purely in terms of surface variables

$$U_t+UU_x+VU_y+\left(a_{11}+\frac{Dw}{Dt}\Big|^h\right)h_x+a_{12}\,h_y=b_1+\sigma\partial_x\mathsf{div}(\boldsymbol{\kappa})\,.\tag{4.3}$$

The coefficients in this equation are

$$\begin{aligned}a_{11}(x,y,t) &= 2\Omega_1 V-(\Omega_1^2+\Omega_2^2)(h+d_3)-\beta\\ &= 2\Omega_1 V+\mathbf{Q}\mathbf{e}_3\cdot\ddot{\mathbf{q}}+g\mathbf{Q}\mathbf{e}_3\cdot\mathbf{e}_3-(\Omega_1^2+\Omega_2^2)(h+d_3)\\ &\quad -(\dot\Omega_2-\Omega_1\Omega_3)(x+d_1)+(\dot\Omega_1+\Omega_3\Omega_2)(y+d_2)\,,\end{aligned}\tag{4.4}$$

$$a_{12}=2\Omega_2 V\,,\tag{4.5}$$

and

$$\begin{aligned}b_1(x,y,t) &= -2\Omega_2 h_t+2\Omega_3 V-\mathbf{Q}\mathbf{e}_1\cdot\ddot{\mathbf{q}}-g\mathbf{Q}\mathbf{e}_1\cdot\mathbf{e}_3+(\Omega_2^2+\Omega_3^2)(x+d_1)\\ &\quad +(\dot\Omega_3-\Omega_1\Omega_2)(y+d_2)-(\dot\Omega_2+\Omega_1\Omega_3)(h+d_3)\,.\end{aligned}\tag{4.6}$$

The use of the unit vectors $\mathbf{e}_1$, $\mathbf{e}_2$ and $\mathbf{e}_3$ is just to compactify notation. The terms with unit vectors are interpreted as follows

$$\mathbf{Q}\mathbf{e}_3\cdot\mathbf{e}_3=Q_{33}\,,$$

where Q_{ij} is the $(i,j)-$th entry of the matrix representation of $\mathbf{Q}$ and

$$\mathbf{Q}\mathbf{e}_3\cdot\ddot{\mathbf{q}}=Q_{13}\ddot q_1+Q_{23}\ddot q_2+Q_{33}\ddot q_3\,,$$

with similar expressions for the other such terms.

A similar argument (see Appendix A.3) leads to the surface $y-$momentum equation

$$V_t+UV_x+VV_y+a_{21}\,h_x+\left(a_{22}+\frac{Dw}{Dt}\Big|^h\right)h_y=b_2+\sigma\partial_y\mathsf{div}(\boldsymbol{\kappa})\,.\tag{4.7}$$

with

$$a_{21}=-2\Omega_1 U\,,\tag{4.8}$$

and

$$\begin{aligned} a_{22} &= -2\Omega_2 U - (\Omega_1^2+\Omega_2^2)(h+d_3) + \mathbf{Q}\mathbf{e}_3\cdot\ddot{\mathbf{q}} + g\mathbf{Q}\mathbf{e}_3\cdot\mathbf{e}_3 \\ &\quad +(\dot\Omega_1+\Omega_2\Omega_3)(y+d_2) - (\dot\Omega_2-\Omega_1\Omega_3)(x+d_1)\,. \end{aligned} \tag{4.9}$$

and

$$\begin{aligned} b_2 &= 2\Omega_1 h_t - 2\Omega_3 U - \mathbf{Q}\mathbf{e}_2\cdot\ddot{\mathbf{q}} - g\mathbf{Q}\mathbf{e}_2\cdot\mathbf{e}_3 + (\Omega_1^2+\Omega_3^2)(y+d_2) \\ &\quad -(\dot\Omega_3+\Omega_1\Omega_2)(x+d_1) + (\dot\Omega_1-\Omega_2\Omega_3)(h+d_3)\,. \end{aligned} \tag{4.10}$$

The terms a_{11} and a_{22} are related by

$$a_{11} - 2\Omega_1 V = a_{22} + 2\Omega_2 U\,.$$

The surface SWEs (4.3) and (4.7) are exact. Moreover the assumption of finite depth has not been used yet and so they are also valid in infinite depth. In order to reduce them to a closed system, the only term that requires modelling is the Lagrangian vertical acceleration at the surface, $\frac{Dw}{Dt}\big|^h$.

5. Penney-Price-Taylor theory for the highest standing wave

Before proceeding to reduce the surface equations to a closed set of shallow water equations a key property of the exact equations is highlighted.

One of the simplest forms of sloshing waves is the pure standing wave. It is periodic in both space and time. Penney & Price (1952) argue that the *highest* standing wave should occur when the Lagrangian vertical acceleration at the crest is equal to $-g$. They consider standing waves in infinite depth only, but it will be clear from the discussion below that their argument is also valid in finite depth. Their argument – in the absence of surface tension – is that the pressure just inside the liquid near the surface must be positive or zero and consequently at the surface $\frac{\partial p}{\partial z} \leqslant 0$ which is equivalent to

$$g + \frac{Dw}{Dt}\bigg|^h \geqslant 0\,. \tag{5.1}$$

When this condition is violated the standing wave should cease to exist. Taking into account that $\frac{Dw}{Dt} = \frac{\partial w}{\partial t}$ at a crest, this is equation (67) in Penney & Price (1952). Using this theory they deduced that the crest angle of the highest wave must be 90^o, in contrast to the 120^o angle of travelling waves. Taylor (1953) was surprised by this argument and tested it by constructing an experiment. He was mainly interesting in the crest angle. His experiments convincingly confirmed the conjecture of Penney & Price (1952).

A theoretical justification of this theory can be deduced from the surface momentum equations. For the case of 2D waves, this argument has been presented in Appendix F of Alemi Ardakani & Bridges (2009*g*). Remarkably this argument carries over to 3D waves. Neglecting surface tension, and assuming the vessel to be stationary, the surface momentum equations (4.3) and (4.7) reduce to

$$\begin{aligned} U_t + UU_x + VU_y + \left(g + \tfrac{Dw}{Dt}\big|^h\right) h_x &= 0 \\ V_t + UV_x + VV_y + \left(g + \tfrac{Dw}{Dt}\big|^h\right) h_y &= 0\,. \end{aligned}$$

When $g + \frac{Dw}{Dt}\big|^h = 0$, these equations reduce to

$$\begin{aligned} U_t + UU_x + VU_y &= 0 \\ V_t + UV_x + VV_y &= 0\,. \end{aligned}$$

These equations are closed and indeed it is shown by Pomeau *et al.* (2008*a*) that they have an exact similarity solution. Moreover this similarity solution gives a form of wave breaking, which has in turn been confirmed by numerical experiments in Pomeau *et al.* (2008*b*). The theoretical argument in Pomeau *et al.* (2008*a*) is by analogy with the shallow water equations but it is shown to be precise in Bridges (2009). This theory indicates that any 3D standing waves will be susceptible to some form of

breaking when the condition (5.1) is violated. Indeed photographs of the experiments of Taylor (1953) show a form of crest instability near the highest standing wave – in the 2D case, and his experiments also show a tendency to 3D near the highest wave. See also Figure 8(c) in Kobine (2008) which shows 3D standing waves reaching a maximum. Adding in surface tension and a rotating frame will add new features to the theory. Surface tension will likely provide a smoothing effect, but rotation will likely lead to a more complicated scenario for breaking.

In this paper we are interested in shallow water sloshing. In this case it is natural to assume that the Lagrangian vertical accelerations at the surface are small, and so we will be working predominantly in the region where the condition (5.1) is strongly satisfied.

6. Conservation of mass

The vertical average of the horizontal velocity is $(\overline{u}(x,y,t),\overline{v}(x,y,t))$ defined by

$$\overline{u} := \frac{1}{h}\int_0^h u(x,y,z,t)\,\mathrm{d}z \quad \text{and} \quad \overline{v} := \frac{1}{h}\int_0^h v(x,y,z,t)\,\mathrm{d}z\,. \tag{6.1}$$

Differentiating

$$\begin{aligned} h_t + (h\overline{u})_x + (h\overline{v})_y &= h_t + h_x u\Big|^h + \textstyle\int_0^h u_x\,\mathrm{d}z + h_y v\Big|^h + \int_0^h v_y\,\mathrm{d}z \\ &= h_t + Uh_x + Vh_y + \textstyle\int_0^h (u_x+v_y+w_z)\,\mathrm{d}z - \int_0^h w_z\,\mathrm{d}z \\ &= h_t + Uh_x + Vh_y - W + w\Big|_{z=0} \\ &= 0\,, \end{aligned}$$

using $u_x + v_y + w_z = 0 = 0$, the bottom boundary condition and the kinematic free surface boundary condition. Hence, if $(\overline{u},\overline{v})$ are used for the horizontal velocity field then the $h-$equation in the SWEs in the form

$$h_t + (h\overline{u})_x + (h\overline{v})_y = 0\,, \tag{6.2}$$

is exact.

However we are interested in an $h-$equation based on the surface horizontal velocity field. The surface and average velocities are related by

$$\begin{aligned} U(x,y,t) - \overline{u}(x,y,t) &= \frac{1}{h}\int_0^h z u_z\,\mathrm{d}z\,, \\ V(x,y,t) - \overline{v}(x,y,t) &= \frac{1}{h}\int_0^h z v_z\,\mathrm{d}z\,. \end{aligned} \tag{6.3}$$

Use these identities to formulate the mass equation in terms of the surface velocity field. Differentiating (6.3) and using mass conservation,

$$\frac{\partial}{\partial x}\left[h(U-\overline{u})\right] + \frac{\partial}{\partial y}\left[h(V-\overline{v})\right] = W + hU_x + hV_y\,.$$

Replace W by the kinematic condition,

$$(h(U-\overline{u}))_x + (h(V-\overline{v}))_y = W + h(U_x+V_y) = h_t + (hU)_x + (hV)_y\,.$$

The error in using the surface velocity field in the $h-$equation can be characterized two ways:

$$W + h(U_x+V_y) \approx 0 \quad \text{or} \quad (h(U-\overline{u}))_x + (h(V-\overline{v}))_y \approx 0\,. \tag{6.4}$$

7. SWEs for 3D sloshing in a rotating vessel

To summarize, the candidate SWEs for (h, U, V) are

$$\begin{aligned} h_t + (hU)_x + (hV)_y &= W + hU_x + hV_y \\ U_t + UU_x + VU_y + \left(a_{11} + \tfrac{Dw}{Dt}\Big|^h \right) h_x + a_{12}\, h_y &= b_1 + \sigma \partial_x \mathsf{div}(\boldsymbol{\kappa}) \\ V_t + UV_x + VV_y + a_{21}\, h_x + \left(a_{22} + \tfrac{Dw}{Dt}\Big|^h \right) h_y &= b_2 + \sigma \partial_y \mathsf{div}(\boldsymbol{\kappa})\,. \end{aligned} \tag{7.1}$$

The equation for W can be added

$$W_t + UW_x + VW_y = \frac{Dw}{Dt}\Big|^h\,. \tag{7.2}$$

The system (7.1) with or without (7.2) is not closed. If $\frac{Dw}{Dt}\Big|^h$ is specified, then the system of four equations (7.1)-(7.2) for (h, U, V, W) is closed. This system of four equations can be further reduced to a system of 3 equations with an additional assumption on the surface vertical velocity.

Henceforth it is assumed that the vertical velocity at the free surface satisfies

$$\big|W + hU_x + hV_y\big| << 1\,, \tag{**SWE-1**}$$

and the Lagrangian vertical acceleration at the free surface satisfies

$$\left|\frac{Dw}{Dt}\Big|^h\right| << |a_{11}| \quad \text{and} \quad \left|\frac{Dw}{Dt}\Big|^h\right| << |a_{22}|\,. \tag{**SWE-2**}$$

The assumption (**SWE-1**) has an alternative characterization as shown in (6.4). For small vessel motion, the second assumption (**SWE-2**) is equivalent to assuming that the Lagrangian vertical accelerations are small compared with the gravitational acceleration, equivalent to (5.1).

Under the assumptions (**SWE-1**) and (**SWE-2**) and under the additional assumption that $\sigma = 0$ (neglect of surface tension), the SWEs are hyperbolic. When $\sigma \neq 0$ they are dispersive, for in that case

$$\mathsf{div}(\boldsymbol{\kappa}) = \frac{\partial \kappa_1}{\partial x} + \frac{\partial \kappa_2}{\partial y} = h_{xx} + h_{yy} + \cdots\,,$$

where the dots correspond to nonlinear terms in h and its derivatives. Hence the σ terms in the right-hand side of (U, V) equations in (7.1) have the form

$$\begin{aligned} \partial_x \mathsf{div}(\boldsymbol{\kappa}) &= h_{xxx} + h_{yyx} + \cdots\,, \\ \partial_y \mathsf{div}(\boldsymbol{\kappa}) &= h_{xxy} + h_{yyy} + \cdots\,. \end{aligned}$$

At the linear level, these terms add dispersion to the SWEs. They will also require additional boundary conditions at the walls (cf. Billingham 2002; Kidambi & Shankar 2004), as a contact angle effect appears at the vessel walls. In this paper we will be primarily concerned with long waves and so will henceforth neglect surface tension:

$$\sigma = 0\,. \tag{**SWE-3**}$$

8. Prescribing the rigid-body motion of the vessel

The fluid vessel is a rigid body free to undergo any motion in 3−dimensional space. Every rigid body motion in $\mathbb{R}^3$ is uniquely determined by $(\mathbf{q}(t), \mathbf{Q}(t))$ where $\mathbf{q}(t)$ is the 3−component translation vector and $\mathbf{Q}(t)$ is an orthogonal matrix with unit determinant (cf. Chapter 7 of O'Reilly 2008). In terms of the body coordinates, the translations are surge, sway and heave, and the rotations are labelled roll, pitch and yaw as illustrated in Figure 2.

Translations are straightforward to prescribe and need no special attention other than to be careful

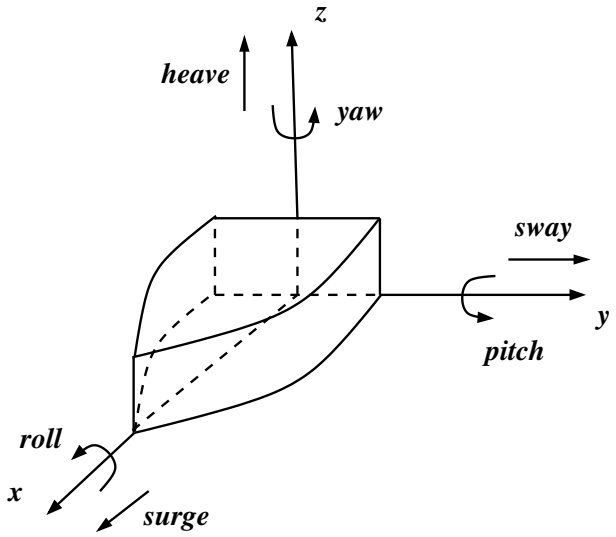

FIGURE 2. Diagram showing conventions for roll, pitch, yaw, surge, sway and heave.

about whether the spatial or body representation is used. In this paper $\mathbf{q}(t)$ is the translation of the body relative to the spatial frame. If the translation is specified from onboard the vessel – that is, specifying the surge, sway and heave directly – then the accelerations are related by

$$\begin{pmatrix} \ddot{q}_1^{surge} \\ \ddot{q}_2^{sway} \\ \ddot{q}_3^{heave} \end{pmatrix} = \begin{bmatrix} Q_{11} & Q_{21} & Q_{31} \\ Q_{12} & Q_{22} & Q_{32} \\ Q_{13} & Q_{23} & Q_{33} \end{bmatrix} \begin{pmatrix} \ddot{q}_1 \\ \ddot{q}_2 \\ \ddot{q}_3 \end{pmatrix} .$$

The natural approach in the context of expermiments is to specify the absolute translations along with the rotations. Although we are not aware of any experiments which combine both. The paper of Disimile *et al.* (2009) indicates that their experimental facility for sloshing has the capability to produce all 6 degrees of freedom in the forcing, but only planar motions are reported so far.

On the other hand specification of the rotations requires some care. The set of orthogonal matrices is highly nonlinear and in $\mathbb{R}^3$ the rotation matrices are no longer commutative in general. The simplest way to specify a rotation is to use Euler angles. However, even here one must be careful because Euler angle representations are inherently singular, and their are subtleties in the deduction of the appropriate angular velocity.

The construction of $\mathbf{Q}(t)$ can also be approached directly using numerical integration. The rotation matrix satisfies the differentiation equation

$$\dot{\mathbf{Q}} = \mathbf{Q}\widehat{\mathbf{\Omega}}\,, \quad \mathbf{Q}(0) = \mathbf{I}\,, \tag{8.1}$$

where $\widehat{\mathbf{\Omega}}$ is the matrix representation of the body angular velocity (2.1). This approach is most effective if the angular velocity is given. One setting where the body angular velocity is available is in strapdown inertial navigation systems (e.g. Chapter 11 of Titterton & Weston 2004). The navigation system outputs the body angular velocity and then (8.1) is solved numerically for $\mathbf{Q}(t)$ (called the attitude matrix in navigation literature).

Another efficient approach to constructing rotation matrices is the use of quaternions. Quaternions are now widely used in computer graphics algorithms (Hanson 2006) and in molecular dynamics (Evans 1977; Rapaport 1985). Evans (1977) points out that "quaternion [computer] programmes seem to run ten times faster than corresponding [computer] programmes employing Euler angles." However in our case the computing time for the rotations is very small compared to the computing time for the fluid motion, so the simpler approach of computing $\mathbf{Q}$ directly by integrating (8.1) is adapted.

The differential equation (8.1) can be integrated numerically very efficiently, although the choice of numerical integrator is very important as it is essential to maintain orthogonality to machine accuracy.

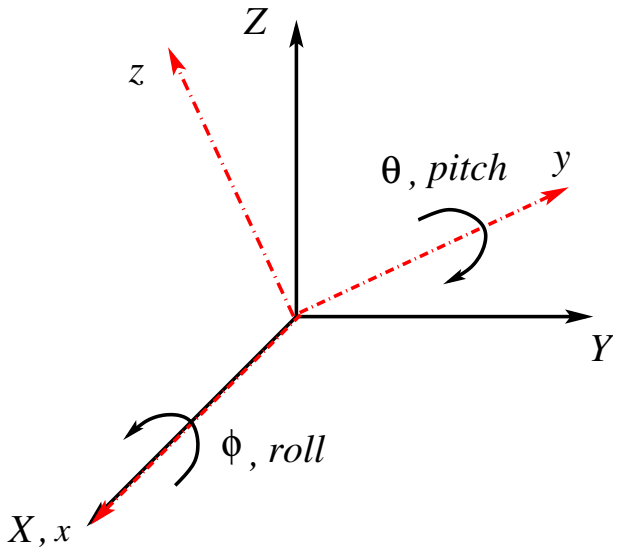

FIGURE 3. Schematic of the roll-pitch motion in terms of Euler angles ϕ and θ.

An efficient second-order algorithm for (8.1) is the implicit midpoint rule (Leimkuhler & Reich 2004) with discretization

$$\frac{\mathbf{Q}^{n+1}-\mathbf{Q}^n}{\Delta t}=\left(\frac{\mathbf{Q}^{n+1}+\mathbf{Q}^n}{2}\right)\widehat{\mathbf{\Omega}}\left(t^{n+\frac{1}{2}}\right),$$

where $\widehat{\mathbf{\Omega}}(t)$ is treated as given; rearranging

$$\mathbf{Q}^{n+1}=\mathbf{Q}^n+\tfrac{1}{2}\Delta t\left(\mathbf{Q}^{n+1}+\mathbf{Q}^n\right)\widehat{\mathbf{\Omega}}\left(t^{n+\frac{1}{2}}\right).$$

Setting

$$\mathbf{S}^{n+\frac{1}{2}}=\tfrac{1}{2}\Delta t\widehat{\mathbf{\Omega}}\left(t^{n+\frac{1}{2}}\right),$$

one time step is represented by

$$\mathbf{Q}^{n+1}=\mathbf{Q}^n\left(\mathbf{I}+\mathbf{S}^{n+\frac{1}{2}}\right)\left(\mathbf{I}-\mathbf{S}^{n+\frac{1}{2}}\right)^{-1}. \tag{8.2}$$

Since $\mathbf{S}^n$ is skew-symmetric, the term $(\mathbf{I}+\mathbf{S}^n)(\mathbf{I}-\mathbf{S}^n)^{-1}$ is orthogonal. Hence orthogonality is preserved to machine accuracy at each time step.

The implicit midpoint rule is a special case of the Gauss-Legendre Runge-Kutta (GLRK) methods which have been shown to preserve orthogonality to machine accuracy, and they can be constructed to any order of accuracy (Leimkuhler & Reich 2004). There are other effective and efficient methods for integrating the equation (8.1) and some recent developments are reviewed in Romero (2008).

8.1. *Euler angles – roll-pitch rotation*

Roll-pitch motion is the simplest non-commutative rotation that is of interest in ship dynamics. The roll-pitch excitation has been used by a number of authors for forced sloshing (e.g. Pantazopoulos 1988, 1987; Faltinsen *et al.* 2006*b*; Huang & Hsiung 1996, 1997; Huang 1995).

In this subsection the properties of the Euler angle representation of roll-pitch are recorded. The roll-pitch rotation consists of a counterclockwise roll rotation about the $x-$axis with angle ϕ, followed by a counterclockwise pitch rotation about the current $y-$axis, as illustrated schematically in Figure 3. After converting both rotations to the same basis the rotation matrix takes the form

$$\mathbf{Q}=\begin{bmatrix}\cos\theta & 0 & \sin\theta\\ \sin\phi\sin\theta & \cos\phi & -\sin\phi\cos\theta\\ -\cos\phi\sin\theta & \sin\phi & \cos\phi\cos\theta\end{bmatrix}. \tag{8.3}$$

From this expression the body representation of the angular velocity is easily deduced using $\mathbf{Q}^T\dot{\mathbf{Q}} = \widehat{\mathbf{\Omega}}$ and so

$$\mathbf{\Omega} = \begin{pmatrix} \dot{\phi}\cos\theta \\ \dot{\theta} \\ \dot{\phi}\sin\theta \end{pmatrix} . \tag{8.4}$$

The spatial angular velocity is obtained by multiplication of $\mathbf{\Omega}$ by $\mathbf{Q}$. A derivation of the roll-pitch angular velocity from first principles is given in Alemi Ardakani & Bridges (2009*d*).

If θ and ϕ are considered as small, then the approximate body angular velocity is

$$\mathbf{\Omega} \approx \left(\dot{\phi}, \dot{\theta}, 0\right) , \tag{8.5}$$

obtained by neglecting quadratic and higher-order terms in (8.4). This simplified version of the angular velocity has been used by Pantazopoulos (1988, 1987), Falzarano *et al.* (2002) and Faltinsen *et al.* (2006*b*). A significant problem with this simplification is that the rotation has been qualitatively changed: the body and spatial represenations are equal and so it behaves like a planar rotation. Secondly, in a numerical context this simplification is not necessary.

8.2. *Yaw-pitch-roll rotation and 3-2-1 Euler angles*

The yaw-pitch-roll rotation is one of the most widely used Euler angle sequences (see §6.8.1 of O'Reilly (2008) where they are called the 3-2-1 Euler angle sequence). It was first used in the context of sloshing by Huang (1995) and Huang & Hsiung (1996, 1997).

The 3-2-1 Euler angle sequence starts with a yaw rotation about the $z-$axis with angle ψ, followed by a pitch rotation about the new $y-$axis denoted by θ, followed by a roll rotation about the new $x-$axis denoted by ϕ. The composite rotation is

$$\mathbf{Q} = \begin{bmatrix} \cos\theta\cos\psi & \sin\phi\sin\theta\cos\psi - \cos\phi\sin\psi & \cos\phi\sin\theta\cos\psi + \sin\phi\sin\psi \\ \cos\theta\sin\psi & \sin\phi\sin\theta\sin\psi + \cos\phi\cos\psi & \cos\phi\sin\theta\sin\psi - \sin\phi\cos\psi \\ -\sin\theta & \sin\phi\cos\theta & \cos\phi\cos\theta \end{bmatrix} . \tag{8.6}$$

The body angular velocity is computed to be

$$\mathbf{\Omega} = \begin{pmatrix} \dot{\phi} - \dot{\psi}\sin\theta \\ \dot{\psi}\cos\theta\sin\phi + \dot{\theta}\cos\phi \\ \dot{\psi}\cos\theta\cos\phi - \dot{\theta}\sin\phi \end{pmatrix} . \tag{8.7}$$

Full details of the 3-2-1 Euler angles and the derivation of the angular velocity are given in Alemi Ardakani & Bridges (2009*c*).

In matrix form the angular velocity is related to the Euler angles by

$$\mathbf{\Omega} = \mathbf{B}^{-1}\dot{\Theta} ,$$

with

$$\mathbf{B} = \begin{bmatrix} 1 & \sin\phi\tan\theta & \cos\phi\tan\theta \\ 0 & \cos\phi & -\sin\phi \\ 0 & \sin\phi\sec\theta & \cos\phi\sec\theta \end{bmatrix} \quad \text{and} \quad \Theta := \begin{pmatrix} \phi \\ \theta \\ \psi \end{pmatrix} .$$

This is the form of the angular velocity used in Huang (1995) and Huang & Hsiung (1997). The singularity of this Euler angle representation arises due to the non-invertibility of $\mathbf{B}$:

$$\det(\mathbf{B}) = \sec\theta ,$$

and so to avoid the singularity the restriction $-\frac{1}{2}\pi < \theta < \frac{1}{2}\pi$ is required. In the context of ship dynamics this is not a severe restriction.

If all three angles are small then $\mathbf{B}$ is approximately the identity and

$$\mathbf{\Omega} \approx \begin{pmatrix} \dot{\phi} \\ \dot{\theta} \\ \dot{\psi} \end{pmatrix} .$$

This approximation is appealing, since then $\mathbf{\Omega} = \dot{\Theta}$ and $\dot{\mathbf{\Omega}} = \ddot{\Theta}$, with $\Theta = (\phi, \theta, \psi)$. But the spatial and body representations are equal, and so the approximate rotation is qualitatively different from the exact rotation. In the numerical setting an approximation is not needed and the exact expression is used.

8.3. *Harmonic forcing*

Harmonic motion can be specified by expressing the Euler angles in terms of harmonic motion. For example in the case of roll-pitch with the same frequency and phase, but different amplitudes,

$$\phi(t) = \varepsilon_1 \cos\omega t \quad \text{and} \quad \theta(t) = \varepsilon_2 \cos\omega t\,.$$

In choosing the forcing frequency it is not the value of the frequency that is important but its value relative to the natural frequency. In the limit of shallow water, the natural frequencies of the fluid are

$$\omega_{mn} = \pi\sqrt{gh_0}\left(\frac{m^2}{L_1^2} + \frac{n^2}{L_2^2}\right)^{1/2}. \tag{8.8}$$

9. Review of previous derivations of rotating SWEs for sloshing

Two derivations of the SWEs for fluid in a vessel that is undergoing a general rigid-body motion in three dimensions first appeared in the literature at about the same time, given independently by Dillingham & Falzarano (1986) and Pantazopoulos (1987). Both derivations follow the same strategy. Their respective derivations are an extension of the formulation for two-dimensional shallow water flow in a rotating frame in Dillingham (1981).

This review of their derivation serves two purposes. It shows how the choice of representation of the angular velocity is very important, and secondly, it shows how the new SWEs in §7 compare with previous work. Hereafter these equations (introduced below in equation (9.2)) will be called the DFP SWEs.

The DFP derivation starts with the classical SWEs

$$\begin{aligned} u_t + uu_x + vu_y + gh_x &= 0 \\ v_t + uv_x + vv_y + gh_y &= 0 \\ h_t + (hu)_x + (hv)_y &= 0\,. \end{aligned} \tag{9.1}$$

Then replace g with the vertical acceleration of the moving frame, and add the horizontal accelerations to the right hand side of the two momentum equations, leading to

$$\begin{aligned} u_t + uu_x + vu_y + a_{(z)}h_x &= f_1 \\ v_t + uv_x + vv_y + a_{(z)}h_y &= f_2 \\ h_t + (hu)_x + (hv)_y &= 0\,, \end{aligned} \tag{9.2}$$

with

$$\begin{aligned} f_1 = {} & -\ddot{n}_1\cos\theta - \ddot{n}_2\sin\phi\sin\theta + \ddot{n}_3\sin\theta\cos\phi - 2\omega_1\omega_2 x\sin\phi\sin\theta\cos\theta \\ & -\omega_1\omega_2 y\cos\phi\cos\theta - \omega_1\omega_2 z_d\sin\phi(\sin^2\theta - \cos^2\theta) + \omega_1^2 x\sin^2\theta \\ & -\omega_1^2 z_d\sin\theta\cos\theta + \omega_2^2 x(1 - \sin^2\theta\sin^2\phi) - \omega_2^2 y\sin\phi\sin\theta\cos\phi \\ & +\omega_2^2 z_d\sin\theta\sin^2\phi\cos\theta + 2\omega_1 v\sin\theta - 2\omega_2 v\sin\phi\cos\theta + \dot{\omega}_1 y\sin\theta \\ & +\dot{\omega}_2 y\sin\phi\cos\theta - \dot{\omega}_2 z_d\cos\phi + g\sin\theta\cos\phi\,, \end{aligned} \tag{9.3}$$

$$\begin{aligned} f_2 = {} & -\ddot{n}_2\cos\phi - \ddot{n}_3\sin\phi + \omega_1^2 y - \omega_2^2 x\sin\phi\sin\theta\cos\phi + \omega_2^2 y\sin^2\phi \\ & +\omega_2^2 z_d\sin\phi\cos\phi\cos\theta - \omega_1\omega_2 x\cos\phi\cos\theta - \omega_1\omega_2 z_d\sin\theta\cos\phi \\ & -2\omega_1 u\sin\theta + 2\omega_2 u\sin\phi\cos\theta - \dot{\omega}_1 x\sin\theta + \dot{\omega}_1 z_d\cos\theta \\ & +\dot{\omega}_2 x\sin\phi\cos\theta + \dot{\omega}_2 z_d\sin\theta\sin\phi - g\sin\phi\,, \end{aligned} \tag{9.4}$$

and the vertical acceleration is

$$\begin{aligned} a_{(z)} \;=\; & \ddot{n}_1 \sin\theta - \ddot{n}_2 \sin\phi\cos\theta + \ddot{n}_3 \cos\phi\cos\theta + \omega_1\omega_2 x \sin\phi(\sin^2\theta - \cos^2\theta) \\ & + \omega_1\omega_2 y \sin\theta\cos\phi - 2\omega_1\omega_2 z_d \sin\phi\sin\theta\cos\theta \\ & + \omega_1^2 x \sin\theta\cos\theta - \omega_1^2 z_d \cos^2\theta - \omega_2^2 x \sin\theta\sin^2\phi\cos\theta \\ & - \omega_2^2 y \sin\phi\cos\phi\cos\theta - \omega_2^2 z_d(1 - \sin^2\phi\cos^2\theta) + 2\omega_1 v\cos\theta \\ & + 2\omega_2 v \sin\phi\sin\theta - 2\omega_2 u\cos\phi + \dot{\omega}_1 y\cos\theta - \dot{\omega}_2 x\cos\phi \\ & + \dot{\omega}_2 y\sin\phi\sin\theta + g\cos\phi\cos\theta\,. \end{aligned} \tag{9.5}$$

The notation follows the original sources, and several typos have been corrected. $\mathbf{n} = (n_1, n_2, n_3)$ in these equations is the same as $\mathbf{q}$ in §2, and $\boldsymbol{\omega} = (\omega_1, \omega_2, \omega_3)$ is the *spatial* representation of the angular velocity. The other terms will be defined shortly.

At first glance this formulation does not look anything like the rotating SWEs proposed in §7. This discrepancy concerned us greatly, and we undertook a careful investigation of the assumptions and properties of the DFP equations. The details of that investigation, including correction of the various typos and omissions, is recorded in the report of Alemi Ardakani & Bridges (2009*d*). Here we will highlight the main features of the derivation leading to (9.2).

Let $\mathbf{X} = (X, Y, Z)$ be coordinates for the fixed spatial frame and let $\mathbf{x} = (x, y, z)$ be coordinates for the body frame. Then DFP use the following relationship between the fixed frame and the moving frame

$$\mathbf{X} = \mathbf{Q}(\mathbf{x} + \mathbf{d}) + \mathbf{n}\,,$$

with $\mathbf{n}$ identified with $\mathbf{q}$ in §2. They impose the following assumptions on $\mathbf{x}$ and $\mathbf{d}$

$$\mathbf{x} = \begin{pmatrix} x \\ y \\ 0 \end{pmatrix}\,, \tag{\textbf{DFP-1}}$$

and

$$\mathbf{d} = \begin{pmatrix} 0 \\ 0 \\ z_d \end{pmatrix}\,. \tag{\textbf{DFP-2}}$$

The implication of assumption (**DFP-1**) is that they are restricting the 3D equations to the plane $z = 0$. The second assumption (**DFP-2**) is just a choice of axis of rotation and could be generalized within the DFP derivation.

The only forcing considered is roll-pitch of the form in §8.1. The rotation matrix is restricted to

$$\mathbf{Q} = \begin{bmatrix} \cos\theta & 0 & \sin\theta \\ \sin\phi\sin\theta & \cos\phi & -\sin\phi\cos\theta \\ -\cos\phi\sin\theta & \sin\phi & \cos\phi\cos\theta \end{bmatrix}\,. \tag{\textbf{DFP-3}}$$

This matrix is given explicitly in equation (6) on page 29 of Pantazopoulos (1987).

A key assumption in these equations is the use of spatial angular velocity rather than body angular velocity and the assumption

$$\omega_3 = 0\,. \tag{\textbf{DFP-4}}$$

This assumption is a curiosity. It is certainly not necessary in a numerical context, and it is inconsistent since the third component of the body angular velocity is not zero.

The body angular velocity and spatial angular velocity are related by

$$\boldsymbol{\Omega} = \mathbf{Q}^T\boldsymbol{\omega} = \begin{pmatrix} \dot{\phi}\cos\theta \\ \dot{\theta} \\ \dot{\phi}\sin\theta \end{pmatrix}\,.$$

Assuming θ and ϕ small gives

$$\boldsymbol{\omega} \approx \begin{pmatrix} \dot{\phi} \\ \dot{\theta} \\ \phi\dot{\theta} \end{pmatrix} \quad \text{and} \quad \Omega \approx \begin{pmatrix} \dot{\phi} \\ \dot{\theta} \\ \theta\dot{\phi} \end{pmatrix} .$$

If we further neglect the quadratic terms $\phi\dot{\theta}$ and $\theta\dot{\phi}$ then the angular velocities reduce to

$$\boldsymbol{\omega} = \boldsymbol{\Omega} = \begin{pmatrix} \dot{\phi} \\ \dot{\theta} \\ 0 \end{pmatrix} .$$

This is the approximation used explicitly by Falzarano *et al.* (2002) and is implicitly used in Pantazopoulos (1988, 1987). Formalizing this assumption

$$\phi \approx 0 \quad \text{and} \quad \theta \approx 0 . \tag{**DFP-5**}$$

However, the development of the DFP SWEs does not invoke assumption (**DFP-5**) until after the equations are derived. With just assumption (**DFP-4**) the spatial and body accelerations are related by

$$\begin{aligned} \Omega_1 &= \omega_1 \cos\theta + \omega_2 \sin\phi \sin\theta \\ \Omega_2 &= \omega_2 \cos\phi \\ \Omega_3 &= \omega_1 \sin\theta - \omega_2 \sin\phi \cos\theta . \end{aligned} \tag{9.6}$$

Using assumption (**DFP-3**) the translation and gravity terms can be expressed using $\mathbf{Q}$,

$$\ddot{\mathbf{n}} \cdot \mathbf{Q}\mathbf{e}_1 = \ddot{n}_1 \cos\theta + \ddot{n}_2 \sin\phi \sin\theta - \ddot{n}_3 \cos\phi \sin\theta ,$$

and

$$g\mathbf{e}_3 \cdot \mathbf{Q}\mathbf{e}_1 = -g \cos\phi \sin\theta .$$

Using these two expressions, (9.6), and some calculation we find that f_1 simplifies to

$$\begin{aligned} f_1 &= -\ddot{\mathbf{n}} \cdot \mathbf{Q}\mathbf{e}_1 + (\Omega_2^2 + \Omega_3^2)x - \Omega_1\Omega_2 y - \Omega_1\Omega_3 z_d \\ &\quad + 2\Omega_3 v - \dot{\Omega}_2 z_d + \dot{\Omega}_3 y - g\mathbf{e}_3 \cdot \mathbf{Q}\mathbf{e}_1 . \end{aligned} \tag{9.7}$$

A similar construction shows that

$$\begin{aligned} f_2 &= -\ddot{\mathbf{n}} \cdot \mathbf{Q}\mathbf{e}_2 + (\Omega_1^2 + \Omega_3^2)y - \Omega_1\Omega_2 x - \Omega_2\Omega_3 z_d \\ &\quad - 2\Omega_3 u + \dot{\Omega}_1 z_d - \dot{\Omega}_3 x - g\mathbf{e}_3 \cdot \mathbf{Q}\mathbf{e}_2 . \end{aligned} \tag{9.8}$$

The simplification in the expressions (9.7) and (9.8) over the original expressions (9.3) and (9.4) is remarkable. The simplification is due first to the use of the body angular velocity and secondly to the explicit use of the rotation operator. These formulae are verified by substitution and the details are given in Alemi Ardakani & Bridges (2009*d*).

The vertical acceleration term can also be simplified to

$$\begin{aligned} a_{(z)} &= \ddot{\mathbf{n}} \cdot \mathbf{Q}\mathbf{e}_3 - (\Omega_1^2 + \Omega_2^2)z_d + \Omega_1\Omega_3 x + \Omega_2\Omega_3 y \\ &\quad + 2\Omega_1 v - 2\Omega_2 u + \dot{\Omega}_1 y - \dot{\Omega}_2 x + g\mathbf{e}_3 \cdot \mathbf{Q}\mathbf{e}_3 . \end{aligned} \tag{9.9}$$

Now that the DFP SWEs look a little more like the surface SWEs in §7 we can compare the two systems.

The velocity field (U, V) is not the same as the velocity field in the DFP SWEs. DFP do not specify exactly which horizontal velocity they use but their $h-$equation becomes exact if the average horizonatal velocity is used. In any case, assume for purposes of comparison that $(U, V) \approx (u, v)$, and

then the coefficients in the two systems can be compared.

$$\begin{aligned}
a_{11} &= a_{(z)} + 2\Omega_2 U - (\Omega_1^2+\Omega_2^2)h - (\dot\Omega_2 - \Omega_1\Omega_3)d_1 + (\dot\Omega_1 + \Omega_2\Omega_3)d_2\\
a_{12} &= a_{12}^{\rm DFP} + 2\Omega_2 V\\
a_{21} &= a_{21}^{\rm DFP} - 2\Omega_1 U\\
a_{22} &= a_{(z)} - 2\Omega_1 V - (\Omega_1^2+\Omega_2^2)h - (\dot\Omega_2 - \Omega_1\Omega_3)d_1 + (\dot\Omega_1 + \Omega_2\Omega_3)d_2\,.
\end{aligned}$$

In the DFP SWEs $a_{12}^{\rm DFP}$ and $a_{21}^{\rm DFP}$ are identically zero but their symbols are included for comparison. The right-hand side coefficient comparison is

$$\begin{aligned}
b_1 &= f_1 - 2\Omega_2 h_t + (\Omega_2^2+\Omega_3^2)d_1 + (\dot\Omega_3 - \Omega_1\Omega_2)d_2 - (\dot\Omega_2 + \Omega_1\Omega_3)h\\
b_2 &= f_2 + 2\Omega_1 h_t + (\Omega_1^2+\Omega_3^2)d_2 - (\dot\Omega_3 + \Omega_1\Omega_2)d_1 + (\dot\Omega_1 - \Omega_2\Omega_3)h
\end{aligned}$$

The d_1 and d_2 error terms are not so important since they could be included in the DFP formulation so they can be discounted. The discrepancy between the two formulations is still quite significant when the rotation field is present. This discrepancy is due to the fact that the DFP SWEs have more assumptions than the surface SWEs.

9.1. *Review of the HH SWEs*

Another strategy for deriving the SWEs for fluid in a vessel that is undergoing a general rigid-body motion in three dimensions has been proposed by Huang (1995) and Huang & Hsiung (1996, 1997). Their derivation is more precise, and starts with the full 3D equations. A detailed report on their derivation is given in Alemi Ardakani & Bridges (2009*e*). Here a sketch of their derivation is given including a comparison with the DFP SWEs and the surface equations in §7. They explicitly take $u(x,y,z,t)$ and $v(x,y,z,t)$ to be independent of z but implicitly they are using the average horizontal velocity field $(\overline{u},\overline{v})$. They neglect the vertical acceleration in general (not just at the free surface) and integrate the vertical pressure gradient, differentiate and then substitute into the horizontal momentum equations. However due to these assumptions extraneous terms appear which require additional assumptions:

$$2\Omega_2 w \approx 0\,,\quad 2\Omega_1 w \approx 0\,,\quad (\Omega_1 v_x - \Omega_2 u_x)h \approx 0\,,\quad (\Omega_1 v_y - \Omega_2 u_y)h \approx 0\,.$$

The rotation matrix $\mathbf{Q}$ is restricted to the yaw-pitch-roll rotation discussed in §8.2, and they use the body angular velocity representation.

Their derivation leads to SWEs of the form

$$\begin{aligned}
u_t + uu_x + vu_y + a_{11}^{HH}h_x &= b_1^{HH}\,,\\
v_t + uv_x + vv_y + a_{22}^{HH}h_y &= b_2^{HH}\,,\\
h_t + (hu)_x + (hv)_y &= 0\,,
\end{aligned}\tag{9.10}$$

where the (u,v) velocity field here should be interpreted as the average velocity field $(\overline{u},\overline{v})$. To compare these HH SWEs with new surface equations, assume that the (U,V) velocity field in the surface equations is equivalent to the velocity field in the HH SWEs, and compare coefficients

$$\begin{aligned}
a_{11}^{HH} &= a_{11} - 2\Omega_2 u\,,\\
a_{22}^{HH} &= a_{22} + 2\Omega_1 v\,,\\
a_{12}^{HH} &= a_{12} - 2\Omega_2 v\,,\\
a_{21}^{HH} &= a_{21} + 2\Omega_1 u\,,\\
b_1^{HH} &= b_1 + 2\Omega_2 h_t + \dot\Omega_2 h\,,\\
b_2^{HH} &= b_2 - 2\Omega_1 h_t - \dot\Omega_1 h\,.
\end{aligned}\tag{9.11}$$

The agreement between the HH SWEs and the surface SWEs is much better than the case of the DFP SWEs but there are still important differences when Ω_1 and Ω_2 are important. One case where

the surface equations and the HH SWEs agree exactly (assuming equivalence of the velocity fields) is when the forcing is pure yaw motion, and numerical experiments on this case are discussed in §12.

10. Numerical algorithm for shallow-water sloshing

The numerical method we propose for simulation of shallow water sloshing in a vehicle undergoing rigid body motion is an extension of the numerical scheme in Alemi Ardakani & Bridges (2009*g*). It is a finite difference scheme, using centered differencing in space. It is fully implicit and has a block-tridiagonal structure. The basic formulation of the algorithm was first proposed by Leendertse (1967) and refined by Abbott and Ionescu and is widely used in computational hydraulics (cf. Abbott 1979). The only new features in the algorithm are extension to include a fully 3D rotation and translation field, and exact implementation of boundary conditions. The fact that the scheme is implicit makes the introduction of rotations straightforward. Some explicit schemes are unstable in the presence of rotation.

The one-dimensional version of the algorithm was used in Alemi Ardakani & Bridges (2009*g*) and the two-dimensional version is just a concatentation of this scheme: the time step is split into two steps and an alternating direction implicit algorithm is used: implicit in $x-$direction and explicit in the $y-$direction in the first half step and explicit in $x-$direction and implicit in the $y-$direction in the second half step. One of the nice properties of the scheme is that the boundary conditions at the walls are implemented exactly, even at the intermediate time steps.

The scheme has numerical dissipation, but the form of the dissipation is similar to the action of viscosity. The truncation error is of the form of the heat equation and so is strongly wavenumber dependent. Moreover the numerical dissipation follows closely the hydraulic structure of the equations. See the technical report of Alemi Ardakani & Bridges (2009*f*) for an analysis of the form of the numerical dissipation. The numerical dissipation is helpful for eliminating transients and spurious high-wavenumber oscillation in the formation of travelling hydraulic jumps.

In contrast, Pantazopoulos (1987) and Pantazopoulos (1988) use Glimm's method. Glimm's method is very effective for treating a large number of travelling hydraulic jumps, but the solutions are discontinuous, and the scheme has problems with mass conservation. Huang & Hsiung (1996, 1997) use flux-vector splitting. This method involves computing eigenvalues of the Jacobian matrices, and is effective for tracking multi-directional characteristics. It appears to be very effective and accurate but is more complicated to implement than the scheme proposed here.

Setting up the equations for this scheme is straightforward and follows the one-dimensional construction in Alemi Ardakani & Bridges (2009*g*), but the details are lengthy. Hence we have given a detailed construction of the algorithm in an internal report (Alemi Ardakani & Bridges 2009*f*) and in this section just the main features are highlighted.

Rewrite the governing equations in a form suitable for the first half-step of the scheme,

$$\begin{aligned}
h_t + h^\star U_x + U^\star h_x + hV_y + Vh_y &= 0 \\
U_t + U^\star U_x + VU_y + 2\Omega_2 Vh_y + 2\Omega_2 h_t & \\
+ \left[\alpha(x,y,t) + 2\Omega_1 V^\star - \left(\Omega_1^2 + \Omega_2^2\right) h^\star\right] h_x &= 2\Omega_3 V - \left(\dot\Omega_2 + \Omega_1\Omega_3\right) h + \widehat\beta(x,y,t) \qquad (10.1)\\
V_t + U^\star V_x + VV_y - 2\Omega_1 U^\star h_x - 2\Omega_1 h_t & \\
+ \left[\alpha(x,y,t) - 2\Omega_2 U - \left(\Omega_1^2 + \Omega_2^2\right) h\right] h_y &= -2\Omega_3 U + \left(\dot\Omega_1 - \Omega_2\Omega_3\right) h + \widetilde\beta(x,y,t)\,,
\end{aligned}$$

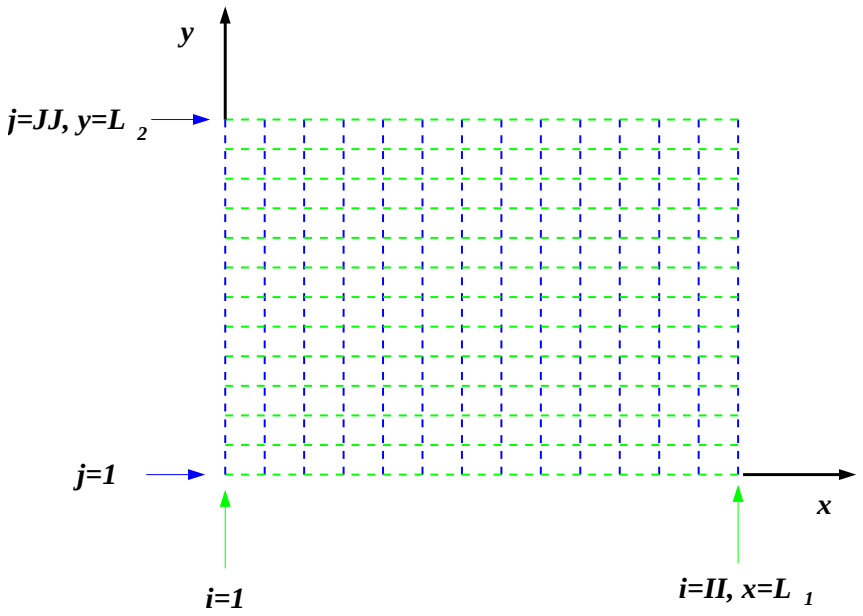

FIGURE 4. A schematic of the grid layout.

where α, $\widehat{\beta}$ and $\widetilde{\beta}$ are the terms that are independent of h, U and V,

$$\begin{aligned}
\alpha(x,y,t) &= -\left(\Omega_1^2+\Omega_2^2\right)d_3+\left(\dot{\Omega}_1+\Omega_2\Omega_3\right)(y+d_2)+\left(\Omega_1\Omega_3-\dot{\Omega}_2\right)(x+d_1)\\
&\quad +\mathbf{Q}\mathbf{e}_3\cdot\ddot{\mathbf{q}}+g\mathbf{Q}\mathbf{e}_3\cdot\mathbf{e}_3\\
\widehat{\beta}(x,y,t) &= -\left(\dot{\Omega}_2+\Omega_1\Omega_3\right)d_3+\left(\dot{\Omega}_3-\Omega_1\Omega_2\right)(y+d_2)+\left(\Omega_2^2+\Omega_3^2\right)(x+d_1)\\
&\quad -\mathbf{Q}\mathbf{e}_1\cdot\ddot{\mathbf{q}}-g\mathbf{Q}\mathbf{e}_1\cdot\mathbf{e}_3\\
\widetilde{\beta}(x,y,t) &= \left(\dot{\Omega}_1-\Omega_2\Omega_3\right)d_3-\left(\dot{\Omega}_3+\Omega_1\Omega_2\right)(x+d_1)+\left(\Omega_1^2+\Omega_3^2\right)(y+d_2)\\
&\quad -\mathbf{Q}\mathbf{e}_2\cdot\ddot{\mathbf{q}}-g\mathbf{Q}\mathbf{e}_2\cdot\mathbf{e}_3\,.
\end{aligned}\tag{10.2}$$

The terms with $\star$ superscript are nonlinear terms that are treated implicitly. In this first half step only $x-$derivatives are implicit and $y-$derivatives are explicit. The nonlinearity is addressed using iteration.

The $x-$interval $0\leqslant x\leqslant L_1$ is split into $II-1$ intervals of length $\Delta x=\frac{L_1}{II-1}$ and so

$$x_i:=(i-1)\Delta x\,,\quad i=1,\ldots,II\,,$$

and the $y-$interval $0\leqslant y\leqslant L_2$ is split into $JJ-1$ intervals of length $\Delta y=\frac{L_2}{JJ-1}$ and so

$$y_j:=(j-1)\Delta y\,,\quad j=1,\ldots,JJ\,,$$

and

$$h^n_{i,j}:=h(x_i,y_j,t_n),\quad U^n_{i,j}:=U(x_i,y_j,t_n)\quad\text{and}\quad V^n_{i,j}:=V(x_i,y_j,t_n)\,,$$

where $t_n=n\Delta t$ with Δt the fixed time step. A schematic of the grid is in Figure 4.

The discretization of the mass equation is

$$\begin{aligned}
&\frac{h^{n+\frac12}_{i,j}-h^n_{i,j}}{\frac12\Delta t}+h^\star_{i,j}\frac{U^{n+\frac12}_{i+1,j}-U^{n+\frac12}_{i-1,j}}{2\Delta x}+U^\star_{i,j}\frac{h^{n+\frac12}_{i+1,j}-h^{n+\frac12}_{i-1,j}}{2\Delta x}\\
&\qquad +h^n_{i,j}\frac{V^n_{i,j+1}-V^n_{i,j-1}}{2\Delta y}+V^n_{i,j}\frac{h^n_{i,j+1}-h^n_{i,j-1}}{2\Delta y}=0\,.
\end{aligned}\tag{10.3}$$

The discretizations of the equations for U, V are

$$\begin{aligned}
&\tfrac{U_{i,j}^{n+\frac12}-U_{i,j}^{n}}{\frac12\Delta t}+U_{i,j}^{\star}\tfrac{U_{i+1,j}^{n+\frac12}-U_{i-1,j}^{n+\frac12}}{2\Delta x}+V_{i,j}^{n}\tfrac{U_{i,j+1}^{n}-U_{i,j-1}^{n}}{2\Delta y}+2\Omega_2^{n+\frac12}V_{i,j}^{n}\tfrac{h_{i,j+1}^{n}-h_{i,j-1}^{n}}{2\Delta y}\\
&\quad+\left[\alpha_{i,j}^{n+\frac12}+2\Omega_1^{n+\frac12}V_{i,j}^{\star}-\left(\left(\Omega_1^{n+\frac12}\right)^2+\left(\Omega_2^{n+\frac12}\right)^2\right)h_{i,j}^{\star}\right]\tfrac{h_{i+1,j}^{n+\frac12}-h_{i-1,j}^{n+\frac12}}{2\Delta x}\\
&=2\Omega_3^{n+\frac12}V_{i,j}^{n+\frac12}-\left(\dot\Omega_2^{n+\frac12}+\Omega_1^{n+\frac12}\Omega_3^{n+\frac12}\right)h_{i,j}^{n+\frac12}-2\Omega_2^{n+\frac12}\tfrac{h_{i,j}^{n+\frac12}-h_{i,j}^{n}}{\frac12\Delta t}+\widehat\beta_{i,j}^{n+\frac12}\\
&\tfrac{V_{i,j}^{n+\frac12}-V_{i,j}^{n}}{\frac12\Delta t}+U_{i,j}^{\star}\tfrac{V_{i+1,j}^{n+\frac12}-V_{i-1,j}^{n+\frac12}}{2\Delta x}+V_{i,j}^{n}\tfrac{V_{i,j+1}^{n}-V_{i,j-1}^{n}}{2\Delta y}-2\Omega_1^{n+\frac12}U_{i,j}^{\star}\tfrac{h_{i+1,j}^{n+\frac12}-h_{i-1,j}^{n+\frac12}}{2\Delta x}\\
&+\left[\alpha_{i,j}^{n+\frac12}-2\Omega_2^{n+\frac12}U_{i,j}^{n}-\left(\left(\Omega_1^{n+\frac12}\right)^2+\left(\Omega_2^{n+\frac12}\right)^2\right)h_{i,j}^{n}\right]\tfrac{h_{i,j+1}^{n}-h_{i,j-1}^{n}}{2\Delta y}\\
&=-2\Omega_3^{n+\frac12}U_{i,j}^{n+\frac12}+\left(\dot\Omega_1^{n+\frac12}-\Omega_2^{n+\frac12}\Omega_3^{n+\frac12}\right)h_{i,j}^{n+\frac12}+2\Omega_1^{n+\frac12}\tfrac{h_{i,j}^{n+\frac12}-h_{i,j}^{n}}{\frac12\Delta t}+\widetilde\beta_{i,j}^{n+\frac12},
\end{aligned}\tag{10.4}$$

where

$$\alpha_{i,j}^{n}:=\alpha(x_i,y_j,t_n),\quad \widehat\beta_{i,j}^{n}:=\widehat\beta(x_i,y_j,t_n)\quad\text{and}\quad \widetilde\beta_{i,j}^{n}:=\widetilde\beta(x_i,y_j,t_n).$$

By setting

$$\mathbf{z}_{i,j}^{n}=\begin{bmatrix}h_{i,j}^{n}\\U_{i,j}^{n}\\V_{i,j}^{n}\end{bmatrix},$$

equations (10.3)-(10.4) can be written in block tridiagonal form

$$\begin{aligned}
-{}_\star\mathbf{A}_{i,j}^{n+\frac12}\mathbf{z}_{i-1,j}^{n+\frac12}+\mathbf{B}^{n+\frac12}\mathbf{z}_{i,j}^{n+\frac12}+{}_\star\mathbf{A}_{i,j}^{n+\frac12}\mathbf{z}_{i+1,j}^{n+\frac12} &= \mathbf{C}_{i,j}^{n+\frac12}\mathbf{z}_{i,j-1}^{n}+\mathbf{D}^{n+\frac12}\mathbf{z}_{i,j}^{n}\\
&\quad-\mathbf{C}_{i,j}^{n+\frac12}\mathbf{z}_{i,j+1}^{n}+\boldsymbol\beta_{i,j}^{n+\frac12}.
\end{aligned}\tag{10.5}$$

The $\star$ left subscript is an indication that the matrix depends on $h^\star$ and/or $U^\star$. Expressions for the matrices are given in (Alemi Ardakani & Bridges (2009*f*)). For fixed $j=2,\dots,JJ-1$ the equations (10.5) are applied for $i=2,\dots,II-1$. To complete the tridiagonal system equations are needed (for each fixed j) at $i=1$ and $i=II$.

10.1. *The equations at $i=1$ and $i=II$ for $j=2,\dots,JJ-1$*

The equations at $i=1$ and $i=II$ are obtained from the boundary conditions at $x=0$ and $x=L_1$. The only boundary condition at $x=0$ is $U(0,y,t)=0$. The discrete version of this is

$$U_{1,j}^{n}=0\quad\text{and}\quad\frac{U_{0,j}^{n}+U_{2,j}^{n}}{2}=0,\quad\text{for each } j,\quad\text{and for all}\quad n\in\mathbb{N}.\tag{10.6}$$

To obtain a boundary condition for h, use the mass equation at $x=0$

$$h_t+h^\star U_x+hV_y+Vh_y=0,$$

with discretization

$$h_{1,j}^{n+\frac12}+\tfrac{\Delta t}{2\Delta x}h_{1,j}^{\star}U_{2,j}^{n+\frac12} = h_{1,j}^{n}-\tfrac{\Delta t}{4\Delta y}h_{1,j}^{n}\left(V_{1,j+1}^{n}-V_{1,j-1}^{n}\right)-\tfrac{\Delta t}{4\Delta y}V_{1,j}^{n}\left(h_{1,j+1}^{n}-h_{1,j-1}^{n}\right).\tag{10.7}$$

To obtain a boundary condition for V, use the $y-$momentum equation at $x=0$

$$V_t+VV_y-2\Omega_1h_t+\left[\alpha(x,y,t)-\left(\Omega_1^2+\Omega_2^2\right)h\right]h_y=\left(\dot\Omega_1-\Omega_2\Omega_3\right)h+\widetilde\beta(x,y,t),$$

with discretization

$$\begin{aligned} V_{1,j}^{n+\frac{1}{2}} - \left[2\Omega_1^{n+\frac{1}{2}} + \tfrac{1}{2}\Delta t\left(\dot{\Omega}_1^{n+\frac{1}{2}} - \Omega_2^{n+\frac{1}{2}}\Omega_3^{n+\frac{1}{2}}\right)\right] h_{1,j}^{n+\frac{1}{2}} &= V_{1,j}^n - \tfrac{\Delta t}{4\Delta y} V_{1,j}^n \left(V_{1,j+1}^n - V_{1,j-1}^n\right) \\ &\quad - \tfrac{\Delta t}{4\Delta y} \widehat{\alpha_{1,j}^{n+\frac{1}{2}}} \left(h_{1,j+1}^n - h_{1,j-1}^n\right) \\ &\quad - 2\Omega_1^{n+\frac{1}{2}} h_{1,j}^n + \tfrac{1}{2}\Delta t \widetilde{\beta}_{1,j}^{n+\frac{1}{2}} , \end{aligned} \tag{10.8}$$

where

$$\widehat{\alpha_{i,j}^n} = \alpha_{i,j}^n - \left(\left(\Omega_1^n\right)^2 + \left(\Omega_2^n\right)^2\right) h_{i,j}^{n-\frac{1}{2}}.$$

Combining equations (10.6), (10.7) and (10.8) gives the equation for $i = 1$

$$\mathbf{E}^{n+\frac{1}{2}} \mathbf{z}_{1,j}^{n+\frac{1}{2}} + {}_\star\mathbf{F}_{1,j} \mathbf{z}_{2,j}^{n+\frac{1}{2}} = \mathbf{G}_{1,j}^{n+\frac{1}{2}} \mathbf{z}_{1,j-1}^n + \mathbf{H}^{n+\frac{1}{2}} \mathbf{z}_{1,j}^n - \mathbf{G}_{1,j}^{n+\frac{1}{2}} \mathbf{z}_{1,j+1}^n +_1 \boldsymbol{\beta}_{1,j}^{n+\frac{1}{2}} . \tag{10.9}$$

Expressions for the matrices are given in Alemi Ardakani & Bridges (2009*f*). A similar strategy is used to construct the discrete equations at $x = L_1$.

10.2. *Summary of the equations for $j = 2, \ldots, JJ-1$*

This completes the construction of the block tridiagonal system at $j-$interior points. For each fixed $j = 2, \ldots, JJ-1$, and fixed $h^\star$, $U^\star$ and $V^\star$, we solve the following block tridiagonal system

$$\begin{aligned} \mathbf{E}^{n+\frac{1}{2}} \mathbf{z}_{1,j}^{n+\frac{1}{2}} + {}_\star\mathbf{F}_{1,j} \mathbf{z}_{2,j}^{n+\frac{1}{2}} &= \mathbf{G}_{1,j}^{n+\frac{1}{2}} \mathbf{z}_{1,j-1}^n + \mathbf{H}^{n+\frac{1}{2}} \mathbf{z}_{1,j}^n \\ &\quad - \mathbf{G}_{1,j}^{n+\frac{1}{2}} \mathbf{z}_{1,j+1}^n +_1 \boldsymbol{\beta}_{1,j}^{n+\frac{1}{2}} , \\ -{}_\star\mathbf{A}_{2,j}^{n+\frac{1}{2}} \mathbf{z}_{1,j}^{n+\frac{1}{2}} + \mathbf{B}^{n+\frac{1}{2}} \mathbf{z}_{2,j}^{n+\frac{1}{2}} + {}_\star\mathbf{A}_{2,j}^{n+\frac{1}{2}} \mathbf{z}_{3,j}^{n+\frac{1}{2}} &= \mathbf{C}_{2,j}^{n+\frac{1}{2}} \mathbf{z}_{2,j-1}^n + \mathbf{D}^{n+\frac{1}{2}} \mathbf{z}_{2,j}^n \\ &\quad - \mathbf{C}_{2,j}^{n+\frac{1}{2}} \mathbf{z}_{2,j+1}^n + \boldsymbol{\beta}_{2,j}^{n+\frac{1}{2}} , \\ -{}_\star\mathbf{A}_{3,j}^{n+\frac{1}{2}} \mathbf{z}_{2,j}^{n+\frac{1}{2}} + \mathbf{B}^{n+\frac{1}{2}} \mathbf{z}_{3,j}^{n+\frac{1}{2}} + {}_\star\mathbf{A}_{3,j}^{n+\frac{1}{2}} \mathbf{z}_{4,j}^{n+\frac{1}{2}} &= \mathbf{C}_{3,j}^{n+\frac{1}{2}} \mathbf{z}_{3,j-1}^n + \mathbf{D}^{n+\frac{1}{2}} \mathbf{z}_{3,j}^n \\ &\quad - \mathbf{C}_{3,j}^{n+\frac{1}{2}} \mathbf{z}_{3,j+1}^n + \boldsymbol{\beta}_{3,j}^{n+\frac{1}{2}} , \\ &\vdots \qquad \vdots \\ -{}_\star\mathbf{F}_{II,j} \mathbf{z}_{II-1,j}^{n+\frac{1}{2}} + \mathbf{E}^{n+\frac{1}{2}} \mathbf{z}_{II,j}^{n+\frac{1}{2}} &= \mathbf{G}_{II,j}^{n+\frac{1}{2}} \mathbf{z}_{II,j-1}^n + \mathbf{H}^{n+\frac{1}{2}} \mathbf{z}_{II,j}^n \\ &\quad - \mathbf{G}_{II,j}^{n+\frac{1}{2}} \mathbf{z}_{II,j+1}^n +_1 \boldsymbol{\beta}_{II,j}^{n+\frac{1}{2}} . \end{aligned} \tag{10.10}$$

Special boundary systems are constructed for the lines $j = 1$ and $j = JJ$. These systems are exactly constructed using boundary conditions and the details are given in Alemi Ardakani & Bridges (2009*f*).

This completes the algorithm details for the first half step $n \mapsto n + \frac{1}{2}$. For each fixed $h^\star$ and $U^\star$, it involves solving a sequence of linear block tridiagonal system for each $j = 1, \ldots, JJ$. Then the process is repeated with updates of $h^\star$ and $U^\star$ till convergence $h^\star \to h^{n+\frac{1}{2}}$ and $U^\star \to U^{n+\frac{1}{2}}$.

The second half step is constructed similarly with $x-$derivatives explicit and $y-$derivatives implicit, and the integration is along vertical grid lines. The details are given in the report of Alemi Ardakani & Bridges (2009*f*).

11. Numerical results: coupled roll-pitch forcing

Suppose the vessel is prescribed to undergo a roll-pitch motion using the Euler angle representation in §8.1. The roll and pitch motions are taken to be harmonic and of the form

$$\phi(t) = \varepsilon_r \sin(\omega_r t) \quad \text{and} \quad \theta(t) = \varepsilon_p \sin(\omega_p t) .$$

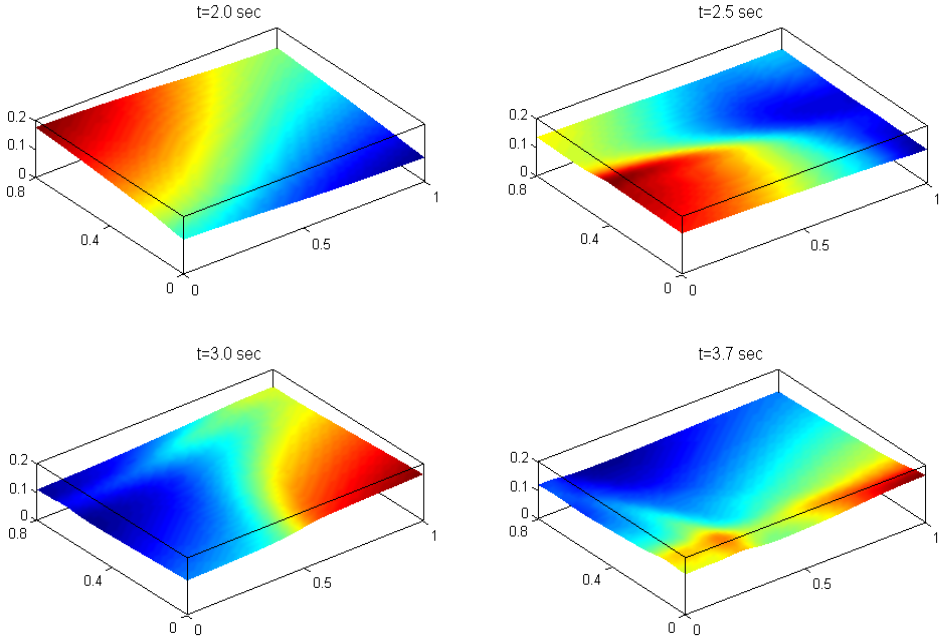

FIGURE 5. Snapshots of free surface profile at a sequence of times for coupled roll-pitch forcing.

The body representation of the angular velocity is then

$$\mathbf{\Omega}(t) = \begin{pmatrix} \varepsilon_r \omega_r \cos(\omega_r t) \cos(\varepsilon_p \sin \omega_p t) \\ \omega_p \varepsilon_p \cos \omega_p t \\ \varepsilon_r \omega_r \cos(\omega_r t) \sin(\varepsilon_p \sin \omega_p t) \end{pmatrix},$$

and the gravity vector is

$$\mathbf{g}(t) := g\mathbf{Q}^T \mathbf{e}_3 = g \begin{pmatrix} -\cos\phi(t)\ \sin\theta(t) \\ \sin\phi(t) \\ \cos\phi(t)\ \cos\theta(t) \end{pmatrix}.$$

The vessel and fluid geometry parameters are set at

$$L_1 = 1.0\,m\,, \quad L_2 = 0.80\,m\,, \quad h_0 = 0.13\,m\,, \quad d_1 = -0.50\,m\,, \quad d_2 = -0.40\,m\,, \quad d_3 = 0.0\,m\,.$$

The numerical parameters are set at

$$\Delta x = 0.02\,m\,, \quad \Delta y = 0.016\,m\,, \quad \Delta t = 0.01\,s\,.$$

Typical CPU time is about 5 seconds per time step without any special optimisation, and a typical run is 500–600 time steps. Simulations are run with quiescent initial conditions: $U = V = 0$ and $h = h_0$ at $t = 0$.

With this fluid geometry, the natural frequencies (8.8) are

$$\omega_{mn} \approx 3.54 \left(m^2 + \frac{n^2}{.64} \right)^{1/2} \ rad/sec\,,$$

with the first two: $\omega_{10} \approx 3.54\,rad/sec$ and $\omega_{01} \approx 4.43\,rad/sec$.

Figures 5 and 6 show snapshots of the free surface at a sequence of times when

$$\varepsilon_p = 1.0^\circ\,, \quad \varepsilon_r = 2.0^\circ\,, \quad \text{and} \quad \omega_p = \omega_r = 2.40\,rad/sec\,.$$

The forcing frequency is much lower than any of the natural frequencies in this case, and the fluid

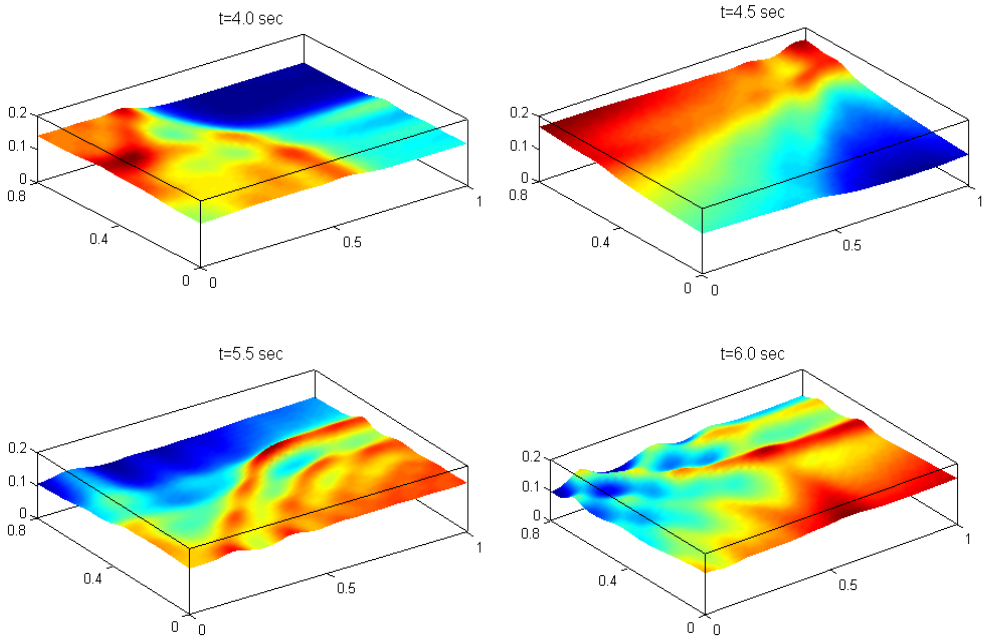

FIGURE 6. Snapshots of free surface in the roll-pitch case: continued.

response is relatively gentle.

Changing the roll and pitch excitation frequency to the natural frequency for each direction,

$$\omega_r = 3.54\, rad/sec \quad \text{and} \quad \omega_p = 4.43\, rad/sec\,,$$

a steep bore forms at $t = 2.0\, sec$ as shown in Figure 7.

Consider now the same amplitudes but a higher frequency

$$\omega_r = \omega_p = 5.60\, rad/sec\,,$$

which is close to the $(1,1)$ natural frequency. A bore is generated and its propagation between the tank's walls is illustrated in Figure 8. The corresponding velocity fields associated with Figure 8 are shown in Figure 9. As can be seen the water particles near the wave fronts have greater speed than in other parts of the tank, and the numerical scheme captures the travelling hydraulic jump very well.

12. Yaw motion and potential vorticity conservation

The case of pure yaw forcing is of interest for several reasons. First, there is a form of potential vorticity conservation; secondly, the surface SWEs and the HH SWEs agree in this case (assuming equal velocity fields) and so the results can be compared, and thirdly this case is the closest to the rotating SWEs in geophysical fluid dynamics.

In the case of pure yaw forcing, the coefficients in the surface SWEs reduce considerably. With $\Omega_1 = \Omega_2 = 0$ and $\Omega_3 = \dot{\psi}$, where $\psi(t)$ is the yaw angle,

$$\begin{aligned} a_{11} &= a_{22} = g\,, \quad a_{12} = a_{21} = 0 \\ b_1 &= 2\Omega_3 V + \Omega_3^2(x + d_1) + \dot{\Omega}_3(y + d_2) \\ b_2 &= -2\Omega_3 U + \Omega_3^2(y + d_2) - \dot{\Omega}_3(x + d_1)\,. \end{aligned}$$

The surface equations and the HH equations are identical (assuming equivalent velocity fields) and

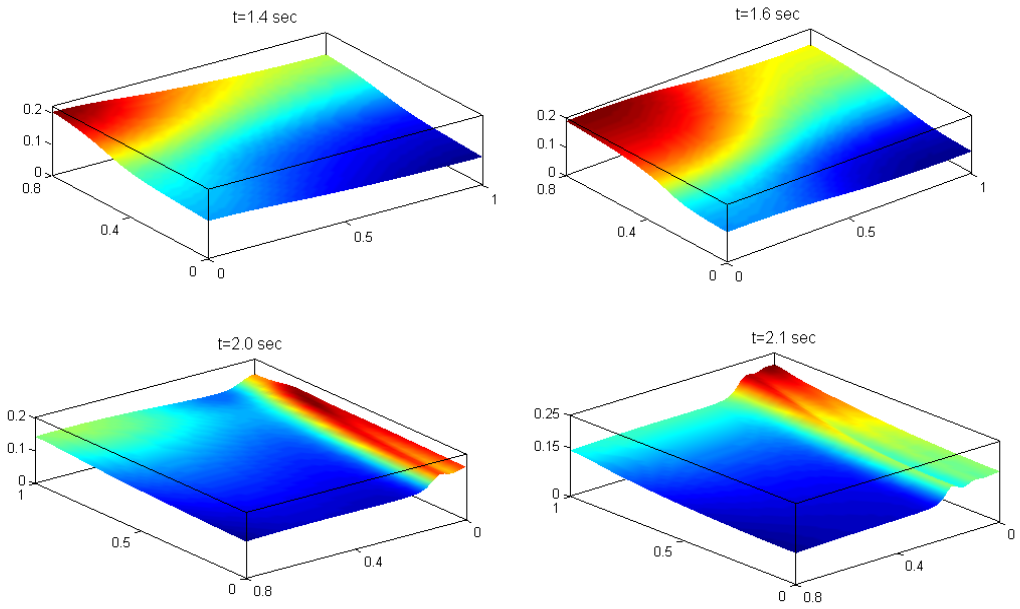

FIGURE 7. Snapshots of free surface profile in the roll-pitch case when the forcing frequency is near the $(1, 0)$ and $(0, 10$ natural frequencies.

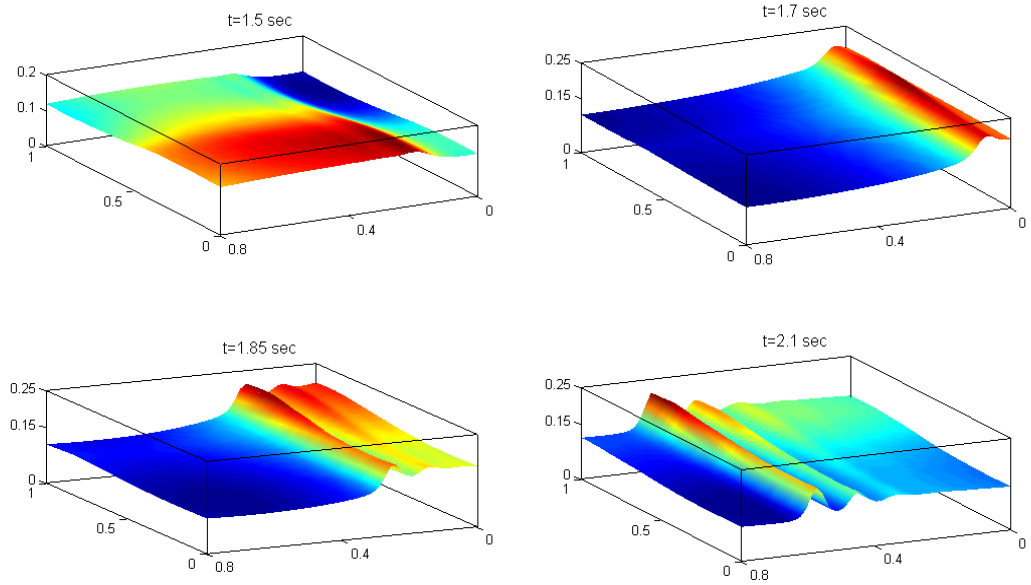

FIGURE 8. Roll-pitch forcing with high frequency, showing formation and propagation of a hydraulic jump.

the momentum equations reduce to the classical SWEs with forcing

$$\begin{aligned} U_t + UU_x + VU_y + gh_x &= 2\dot{\psi}V + \dot{\psi}^2(x + d_1) + \ddot{\psi}(y + d_2) \\ V_t + UV_x + VV_y + gh_y &= -2\dot{\psi}U + \dot{\psi}^2(y + d_2) - \ddot{\psi}(x + d_1)\,. \end{aligned} \tag{12.1}$$

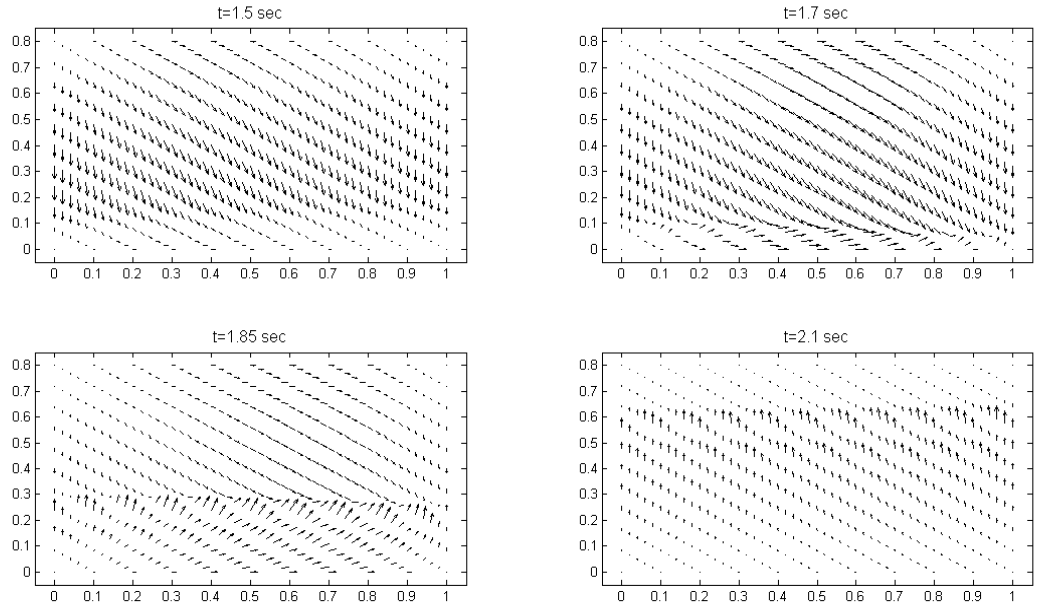

FIGURE 9. Field of velocity vectors associated with the roll-pitch motion in Figure 8.

These equations conserve a form of potential vorticity. Let

$$\mathsf{PV} := \frac{V_x - U_y + 2\dot{\psi}}{h}\,.$$

Then differentiating and using (12.1) shows that

$$\frac{D^{\rm horz}}{Dt}\mathsf{PV} := \frac{\partial}{\partial t}\mathsf{PV} + U\frac{\partial}{\partial x}\mathsf{PV} + V\frac{\partial}{\partial y}\mathsf{PV} = 0\,,$$

and so PV is a Lagrangian invariant for the SWEs (12.1).

Consider the yaw motion to be harmonic

$$\psi\,(t) = \varepsilon_y \sin\,(\omega_y t)\ , \tag{12.2}$$

with parameters

$$\varepsilon_y = 10.0^\circ\,, \quad \text{and} \quad \omega_y = 4.1746\ rad/sec\,.$$

Set the vessel and fluid parameters at

$$L_1 = 1.0\,m\,, \quad L_2 = 1.0\,m\,, \quad h_0 = 0.18\,m\,, \quad d_1 = -0.5\,m\,, \quad d_2 = -0.5\,m\,, \quad d_3 = -0.3\,m\,.$$

The numerical parameters are set at

$$\Delta x = \Delta y = 0.02\,m\,, \quad \text{and} \quad \Delta t = 0.01\,s\,.$$

The forcing frequency is near the lowest natural frequency. The natural frequencies are

$$\omega_{mn} \approx 4.1746\,\sqrt{m^2+n^2}\ rad/sec\,.$$

Snapshots of the surface profile at different values of time are depicted in Figures 10 and 11. There is a very clear swirling motion set up. The corresponding velocity fields associated with Figure 11 are depicted in Figure 12. Here we start to see evidence of a vorticity field. It is predominantly due to the input into the vorticity by the yaw rotation, but this vorticity is enhanced due to the presence of viscous-like truncation error in the numerical scheme.

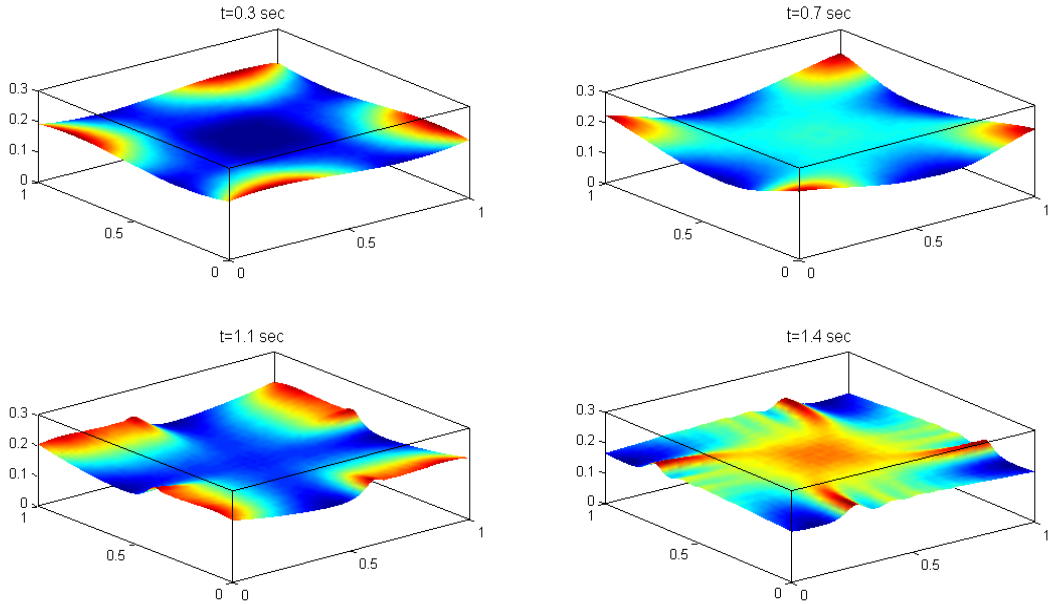

FIGURE 10. Snapshots of surface profile due to yaw forcing.

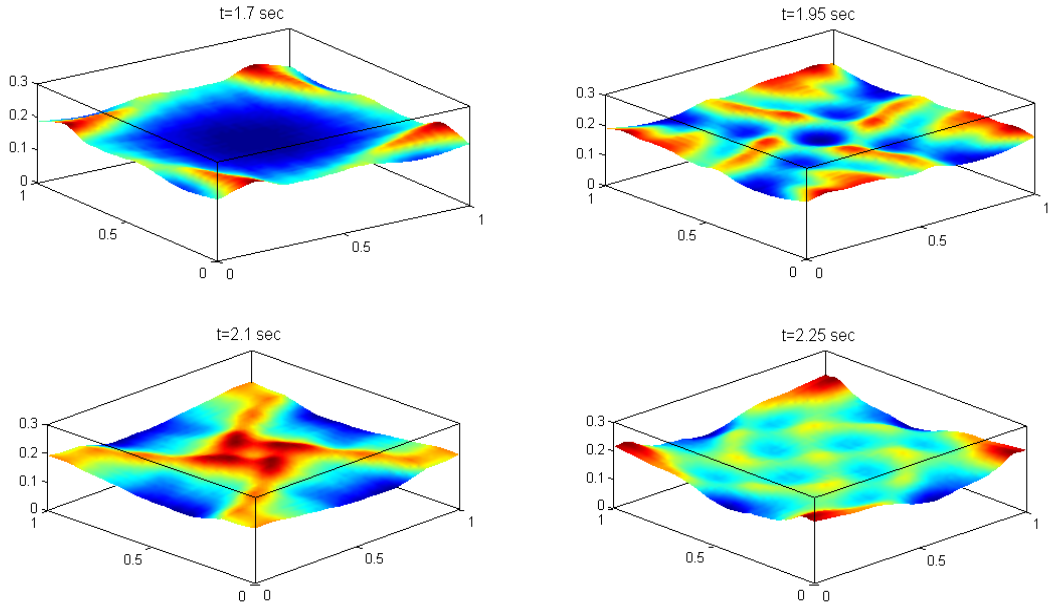

FIGURE 11. Snapshots of surface profile due to yaw forcing: continued.

12.1. *Comparison with results of Huang & Hsiung (1996)*

Now change the parameters in order to compare with the results of Huang & Hsiung (1996). Set the vessel and fluid parameters at

$$L_1 = 1.0\,m\,, \quad L_2 = 0.8\,m\,, \quad h_0 = 0.1\,m\,, \quad d_1 = -0.5\,m\,, \quad d_2 = -0.4\,m\,, \quad d_3 = 0.0\,m\,.$$

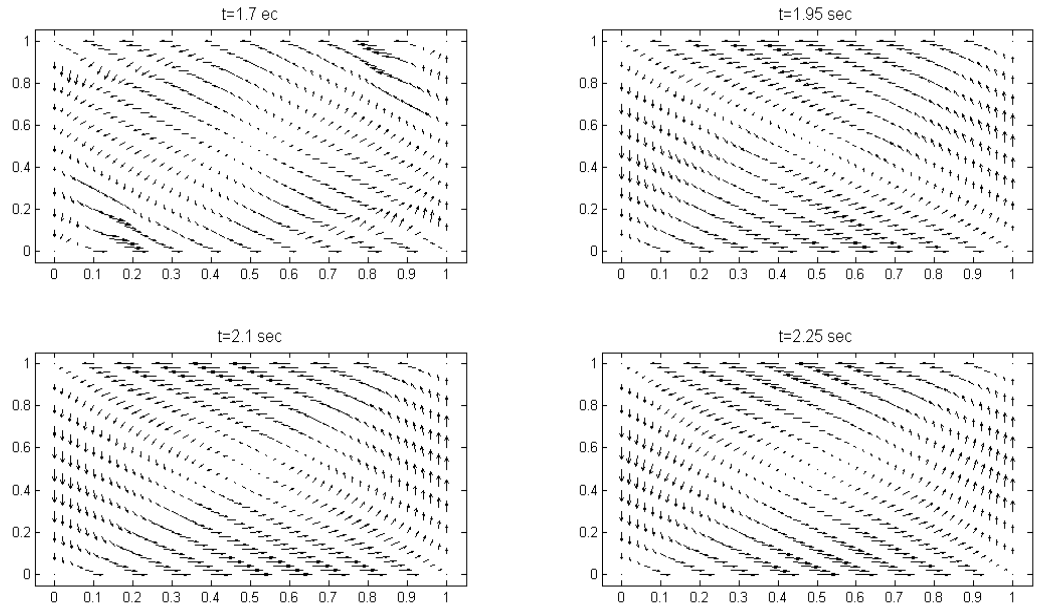

FIGURE 12. Velocity fields associated with Figure 11.

The numerical parameters are

$$\Delta x = 0.02\,m\,, \quad \Delta y = 0.016\,m\,, \quad \Delta t = 0.01\,s\,.$$

The forcing is harmonic yaw motion as in (12.2) with parameters

$$\varepsilon_y = 4.0^\circ\,, \quad \omega_y = 6.0\,rad/sec\,.$$

The snapshot of the surface profile at $t = 1.5\,s$ and the corresponding velocity field are depicted in Figure 13. This result agrees very well with Figure 28 of Huang & Hsiung (1996), including the vortex pattern. The initial conditions are vorticity free. Hence the generation of vorticity is due to the imposed rotation, but it appears to be enhanced by the numerical dissipation.

13. Numerical results: coupled surge-sway motion

Suppose the rotation is zero and the motion undergoes pure translation in the x and y directions. These surge and sway motions are considered to be harmonic

$$q_1\,(t) = \varepsilon_1 \cos\,(\omega_1 t) \quad \text{and} \quad q_2\,(t) = \varepsilon_2 \cos\,(\omega_2 t)\ ,$$

with

$$\varepsilon_1 = \varepsilon_2 = 0.004602\,m\,, \quad \omega_1 = \omega_2 = 4.8006\,rad/sec\,.$$

Set the vessel and fluid aspect ratio parameters at

$$L_1 = 0.59\,m\,, \quad L_2 = 0.59\,m\,, \quad h_0 = 0.2997\,m\,.$$

The offset $\mathbf{d} = 0$ since there is no rotation. The numerical parameters are set at

$$\Delta x = \Delta y = 0.0196\,m\,, \quad \Delta t = 0.01\,s\,.$$

The forcing frequency is chosen to be very near the natural frequency of the exact (not SWE) lowest natural frequency

$$\omega_{10} \approx 1.008\sqrt{g\pi\,\tanh(\pi h_0)}\,.$$

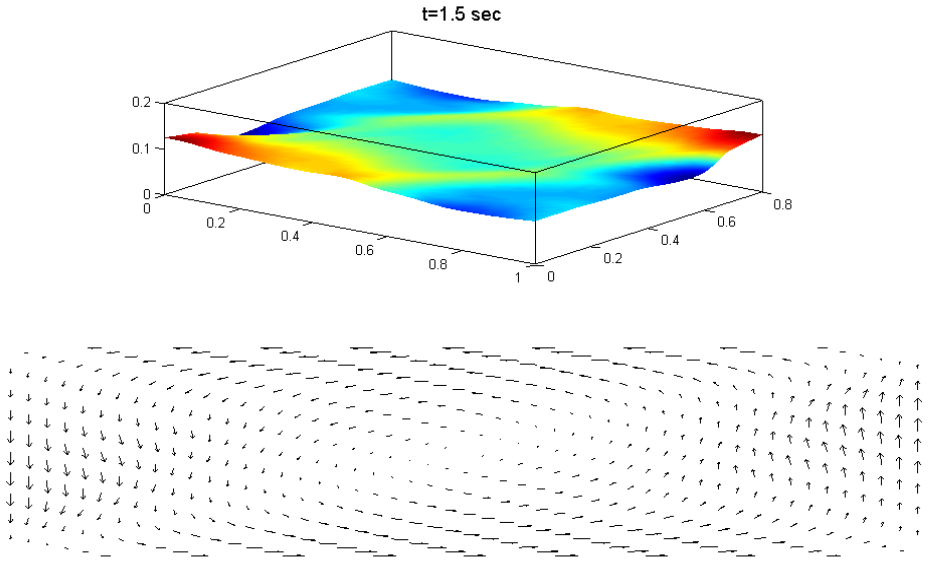

FIGURE 13. Surface profile and velocity field due to yaw at $t = 1.5\,s$: comparison of the numerics based on the surface SWEs with Figure 28 of Huang & Hsiung (1996).

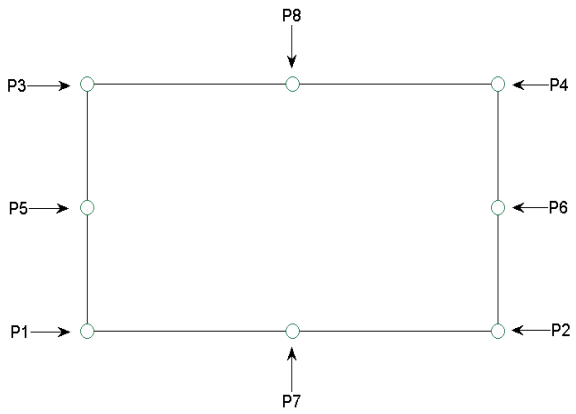

FIGURE 14. Location of the points P_1 to P_8 in the tank cross section.

Particular points are chosen on the vessel cross-section in order to show time histories. This approach is inspired by the simulations of Wu & Chen (2009). The points are labelled as shown in Figure 14. The sloshing histories of surface displacements at points P_1, P_2, P_4 and P_7 are depicted in Figure 15.

The parametric graphs are depicted in Figure 16 showing the presence of square-like waves in the tank.

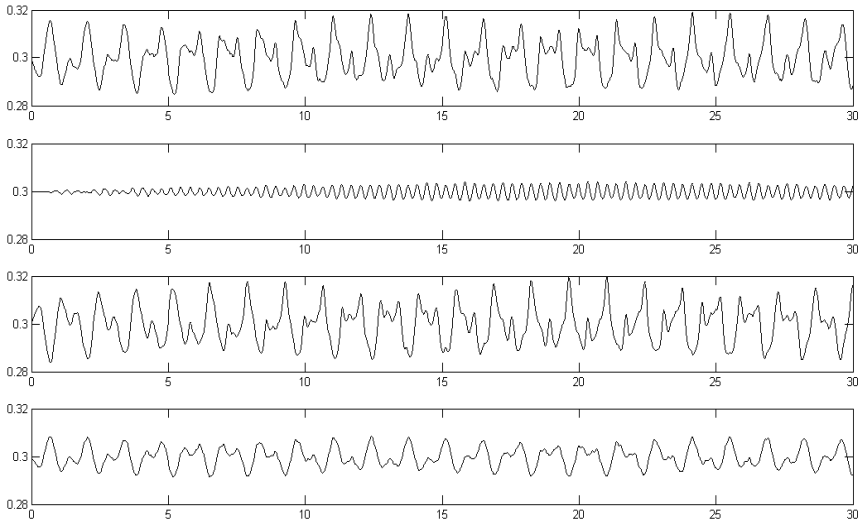

FIGURE 15. Sloshing histories of surface displacements at points P_1 (uppermost plot), P_2, P_4 and P_7 (lowest plot). The horizontal axis is time in seconds, and vertical axis is wave height in meters.

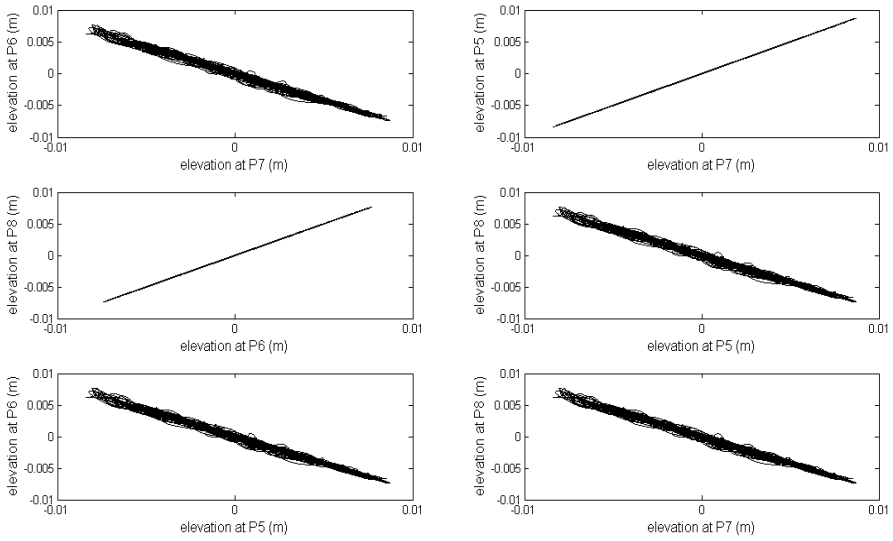

FIGURE 16. Parametric graphs.

Changing the forcing parameters to

$$\varepsilon_1 = 0.0236\, m\,, \quad \varepsilon_2 = 0.0020647\, m\,,$$

and

$$\omega_1 = \omega_2 = 4.7482\, rad/sec\,.$$

These frequencies are close to lowest natural frequency of the full system (rather than the SWE natural frequency)

$$\omega_{10} \approx 0.997\sqrt{g\pi \tanh(\pi h_0)}\,.$$

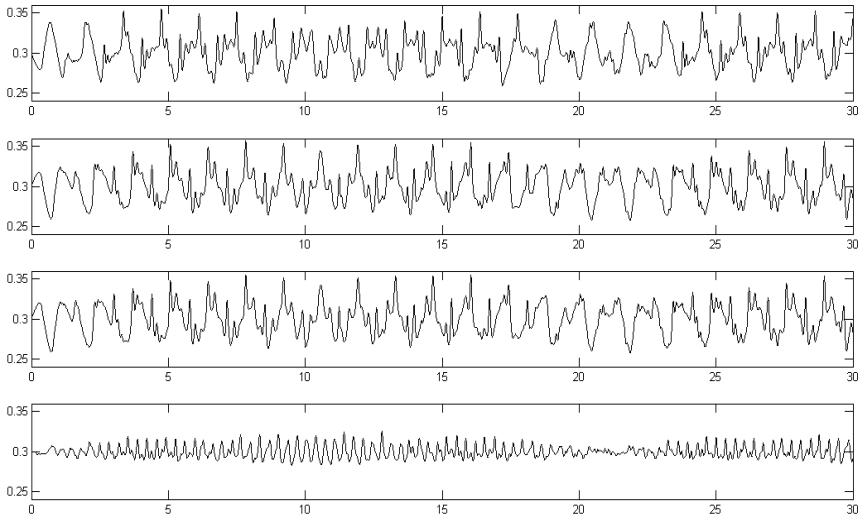

FIGURE 17. Time histories of the surface displacements at points P_1 (upper plot), P_2, P_4 and P_7 (lower plot). The horizontal axis is time in seconds, and vertical axis is wave height in meters.

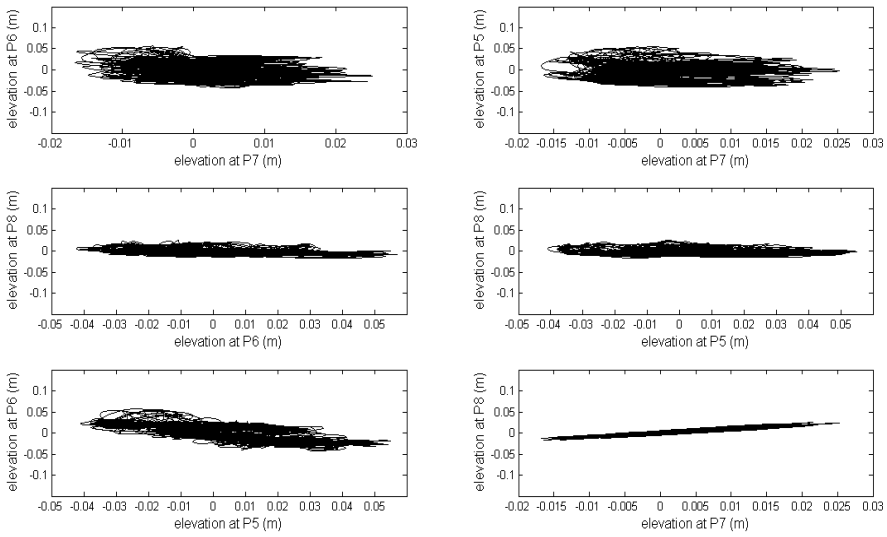

FIGURE 18. Parametric graphs.

The time histories of surface displacements at points P_1, P_2, P_4 and P_7 are depicted in Figure 17.

Further parametric graphs are depicted in Figure 18 showing the presence of planar waves in the tank.

Snapshots of the surface profile at different times are depicted in Figures 19 and 20.

14. Numerical results: coupled yaw-pitch-roll motion

The vessel motion is simulated using the 3-2-1 Euler angles introduced in §8.2. The expression for **Q** is given in equation (8.6) and the required body represenation of the angular velocity is given in

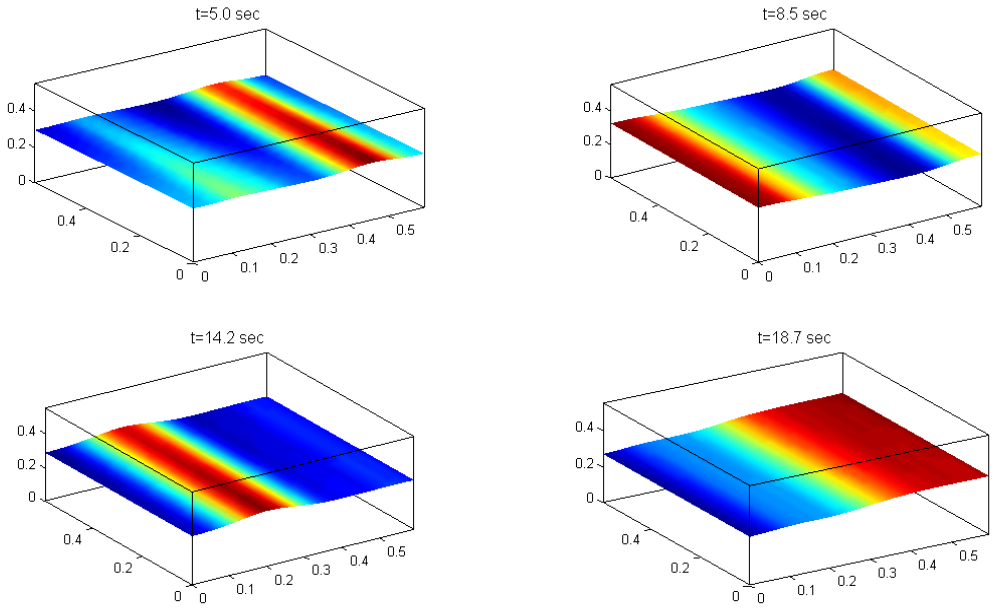

FIGURE 19. Snapshots of surface profile due to surge and sway.

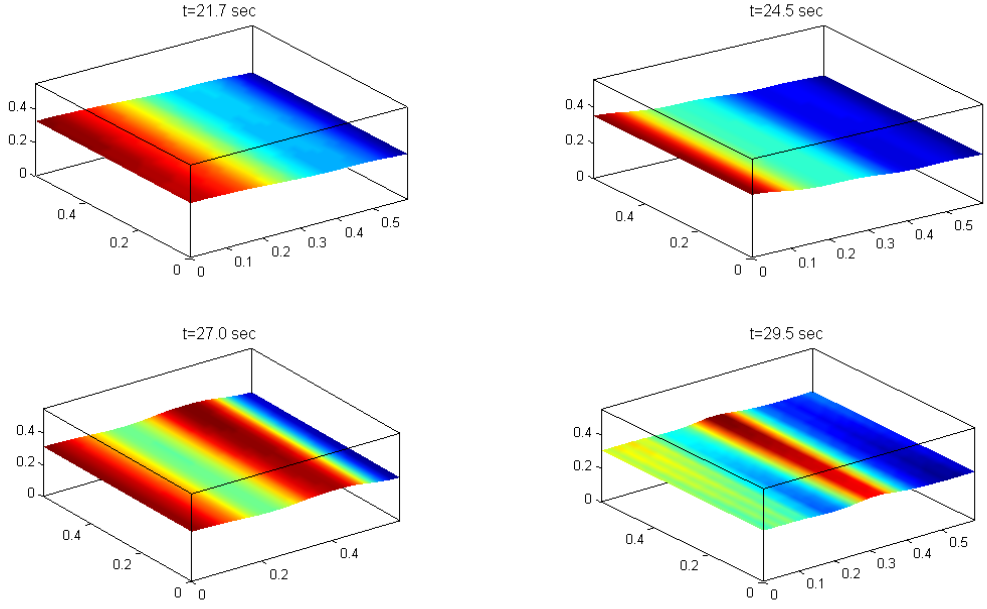

FIGURE 20. Snapshots of surface profile due to surge and sway: continued.

(8.7). The yaw, pitch and roll angles are taken to be harmonic

$$\psi(t) = \varepsilon_y \sin(\omega_y t) \ , \quad \theta(t) = \varepsilon_p \sin(\omega_p t) \ , \quad \phi(t) = \varepsilon_r \sin(\omega_r t) \ .$$

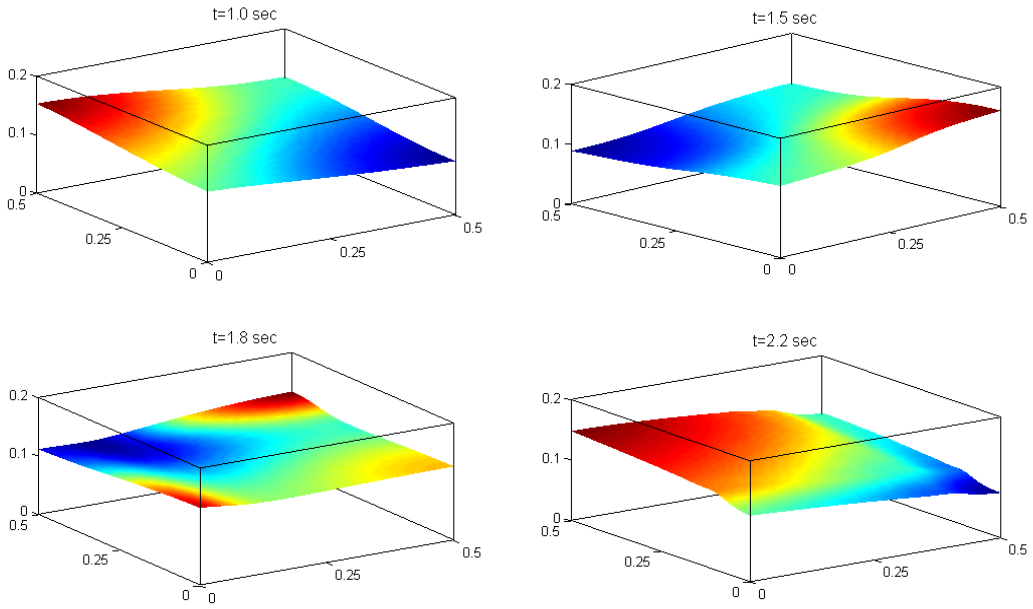

FIGURE 21. Snapshots of surface profile due to roll, pitch and yaw.

The gravity vector is

$$\mathbf{g}(t) := g\mathbf{Q}^T\mathbf{e}_3 = g\begin{pmatrix} -\sin\theta(t) \\ \sin\phi(t)\cos\theta(t) \\ \cos\phi(t)\cos\theta(t) \end{pmatrix}.$$

Set the fluid and vessel geometry parameters at

$$L_1 = 0.50\,m\,, \quad L_2 = 0.50\,m\,, \quad h_0 = 0.12\,m\,, \quad d_1 = -0.25\,m\,, \quad d_2 = -0.25\,m\,, \quad d_3 = 0.0\,m\,.$$

With this geometry the natural frequencies are

$$\omega_{mn} \approx 6.82\sqrt{m^2+n^2}\ rad/sec\,.$$

We will present results for a typical run in this configuration. Take the forcing function parameters to be

$$\varepsilon_y = 2.0^\circ\,, \quad \varepsilon_p = 1.0^\circ\,, \quad \varepsilon_r = 1.0^\circ\,, \quad \omega_y = \omega_p = \omega_r = 5.2171\ rad/sec\,,$$

and set the numerical parameters at

$$\Delta x = \Delta y = 0.01\,m \quad \text{and} \quad \Delta t = 0.01\,s\,.$$

With this low amplitude of forcing the singularity of the Euler angles is safely avoided. About 5.4 seconds of CPU time per required per time step, and simulations were run for about 600 time steps.

Snapshots of the surface profile at a sequence of times are depicted in Figures 21 to 23.

15. Concluding remarks

A new set of shallow water equations which model the three-dimensional rigid body motion of a vessel containing fluid has been derived. The only assumptions are on the vertical velocity and acceleration at the surface. The equations give new insight into shallow water sloshing, include the effect of viscosity, and numerical simulations are much faster than the full 3D equations. The equations capture many of the features of 3D sloshing for the case when the free surface is single valued.

In this paper the vessel motion has been prescribed. The vessel motion can also be determined by

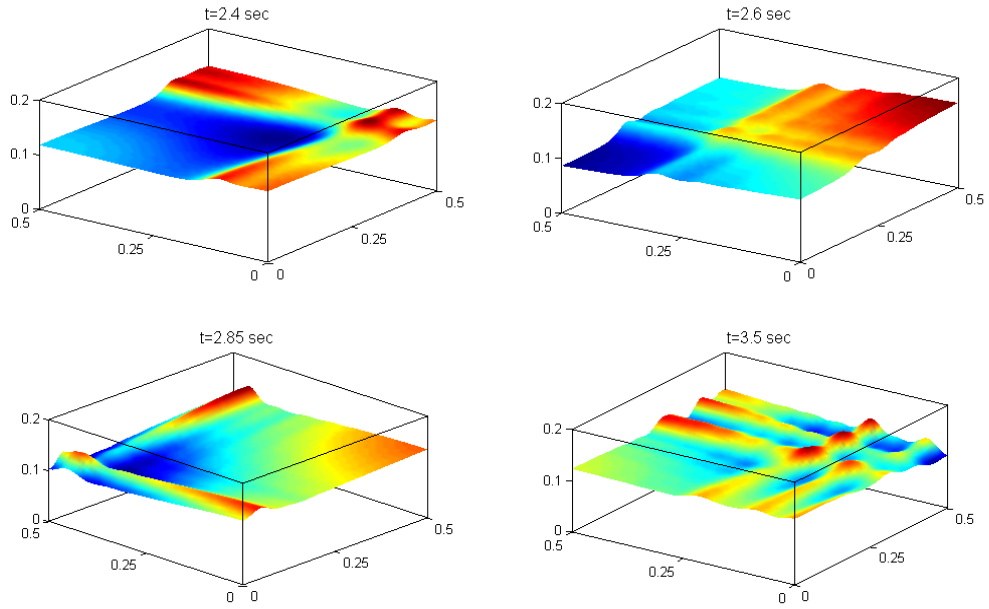

FIGURE 22. Snapshots of surface profile due to roll, pitch and yaw: continued.

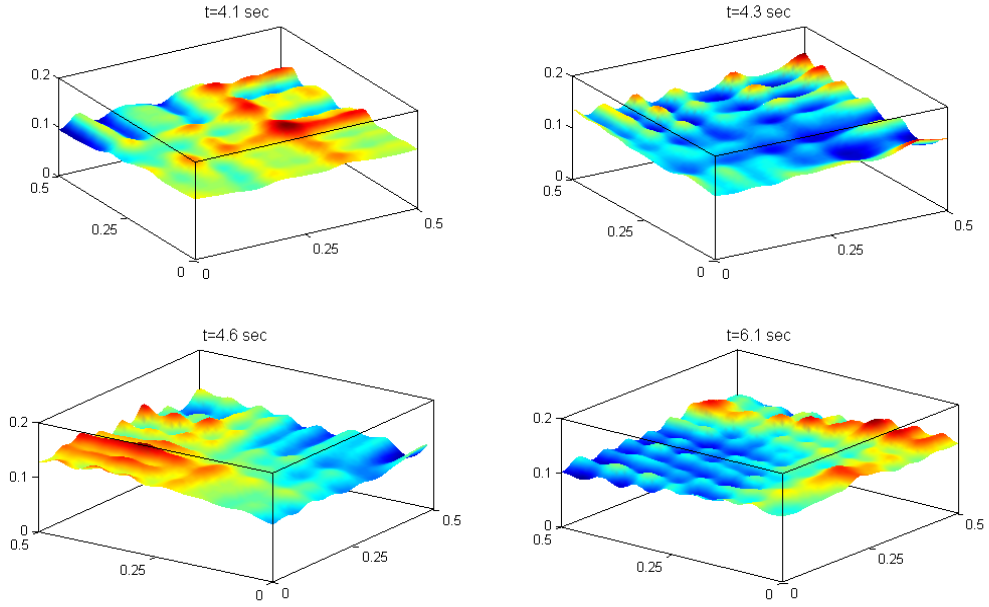

FIGURE 23. Snapshots of surface profile due to roll, pitch and yaw: continued.

solving the rigid body equations coupled to the fluid motion. Some results, for the case of coupled motion for a rigid body with shallow water fluid in two dimensions, have recently been obtained (Alemi Ardakani & Bridges 2009*b*,*a*). The extension to coupling between three-dimensional rigid body motion and shallow water sloshing is however a big step due to the nature of rotations in 3D. The equations of 3D rigid body motion coupled to sloshing have been derived by Veldman *et al.* (2007) for the case

of sloshing in spacecraft. However, simulation in this case is very time consuming. The new surface SWEs introduced here represent the vehicle motion exactly, and therfore provide an opportunity for more efficient simulation of the coupling between the vehicle motion and 3D shallow water sloshing.

— Appendix —

Appendix A. The horizontal pressure gradient

A.1. *x−derivative of pressure*

Differentiate (3.2) with respect to x

$$\begin{aligned}\frac{1}{\rho}\frac{\partial p}{\partial x} &= h_x \tfrac{Dw}{Dt}\Big|^h + \int_z^h \left(\tfrac{Dw}{Dt}\right)_x \mathrm{d}s \\ &\quad +2\Omega_1 V h_x + 2\Omega_1 \int_z^h v_x \,\mathrm{d}s - 2\Omega_2 U h_x - 2\Omega_2 \int_z^h u_x \,\mathrm{d}s \\ &\quad -(\Omega_1^2+\Omega_2^2)(h+d_3)h_x - \beta_x(h-z) - \beta h_x - \sigma\partial_x \mathsf{div}(\boldsymbol{\kappa})\,.\end{aligned}$$

Use the vorticity equation to substitute for $\left(\frac{Dw}{Dt}\right)_x$

$$\begin{aligned}\frac{1}{\rho}\frac{\partial p}{\partial x} &= h_x \tfrac{Dw}{Dt}\Big|^h + \int_z^h \left[\left(\tfrac{Du}{Dt}\right)_z - 2\Omega_1\tfrac{\partial v}{\partial x} - 2\Omega_2\tfrac{\partial v}{\partial y} - 2\Omega_3\tfrac{\partial v}{\partial z} + 2\dot{\Omega}_2\right]\mathrm{d}s \\ &\quad +2\Omega_1 V h_x + 2\Omega_1 \int_z^h v_x \,\mathrm{d}s - 2\Omega_2 U h_x - 2\Omega_2 \int_z^h u_x \,\mathrm{d}s \\ &\quad -(\Omega_1^2+\Omega_2^2)(h+d_3)h_x - \beta_x(h-z) - \beta h_x - \sigma\partial_x \mathsf{div}(\boldsymbol{\kappa})\,.\end{aligned}$$

or

$$\begin{aligned}\frac{1}{\rho}\frac{\partial p}{\partial x} &= h_x \tfrac{Dw}{Dt}\Big|^h + \tfrac{Du}{Dt}\Big|_z^h - 2\Omega_1\int_z^h v_x\,\mathrm{d}s - 2\Omega_2\int_z^h v_y\,\mathrm{d}s - 2\Omega_3\int_z^h v_z\,\mathrm{d}s + 2\dot{\Omega}_2(h-z) \\ &\quad +2\Omega_1 V h_x + 2\Omega_1 \int_z^h v_x \,\mathrm{d}s - 2\Omega_2 U h_x - 2\Omega_2 \int_z^h u_x \,\mathrm{d}s \\ &\quad -(\Omega_1^2+\Omega_2^2)(h+d_3)h_x - \beta_x(h-z) - \beta h_x - \sigma\partial_x \mathsf{div}(\boldsymbol{\kappa})\,.\end{aligned}$$

or

$$\begin{aligned}\frac{Du}{Dt} + \frac{1}{\rho}\frac{\partial p}{\partial x} &= \tfrac{Du}{Dt}\Big|^h + \tfrac{Dw}{Dt}\Big|^h h_x + 2\Omega_2 W - 2\Omega_3 V + 2\dot{\Omega}_2(h-z) \\ &\quad +2\Omega_1 V h_x - 2\Omega_2 U h_x - 2\Omega_2 w + 2\Omega_3 v \\ &\quad -(\Omega_1^2+\Omega_2^2)(h+d_3)h_x - \beta_x(h-z) - \beta h_x - \sigma\partial_x \mathsf{div}(\boldsymbol{\kappa})\,,\end{aligned} \tag{A-1}$$

which is equation (3.3) in §3.

A.2. *y−derivative of pressure*

Differentiate (3.2) with respect to y

$$\begin{aligned}\frac{1}{\rho}\frac{\partial p}{\partial y} &= h_y \tfrac{Dw}{Dt}\Big|^h + \int_z^h \left(\tfrac{Dw}{Dt}\right)_y \mathrm{d}s \\ &\quad +2\Omega_1 V h_y + 2\Omega_1 \int_z^h v_y \,\mathrm{d}s - 2\Omega_2 U h_y - 2\Omega_2 \int_z^h u_y \,\mathrm{d}s \\ &\quad -(\Omega_1^2+\Omega_2^2)(h+d_3)h_y - \beta_y(h-z) - \beta h_y - \sigma\partial_y \mathsf{div}(\boldsymbol{\kappa})\,.\end{aligned}$$

Use the vorticity equation to substitute for $\left(\frac{Dw}{Dt}\right)_x$

$$\begin{aligned}\frac{1}{\rho}\frac{\partial p}{\partial y} &= h_y \tfrac{Dw}{Dt}\Big|^h + \int_z^h \left[\left(\tfrac{Dv}{Dt}\right)_z + 2\Omega_1\tfrac{\partial u}{\partial x} + 2\Omega_2\tfrac{\partial u}{\partial y} + 2\Omega_3\tfrac{\partial u}{\partial z} - 2\dot\Omega_1\right] \mathrm{d}s \\ &\quad +2\Omega_1 V h_y + 2\Omega_1\int_z^h v_y\,\mathrm{d}s - 2\Omega_2 U h_y - 2\Omega_2\int_z^h u_y\,\mathrm{d}s \\ &\quad -(\Omega_1^2+\Omega_2^2)(h+d_3)h_y - \beta_y(h-z) - \beta h_y - \sigma\partial_y \mathsf{div}(\boldsymbol{\kappa})\,.\end{aligned}$$

or

$$\begin{aligned}\frac{1}{\rho}\frac{\partial p}{\partial y} &= h_y \tfrac{Dw}{Dt}\Big|^h + \left(\tfrac{Dv}{Dt}\right)\Big|_z^h + 2\Omega_1\int_z^h u_x\,\mathrm{d}s + 2\Omega_2\int_z^h u_y\,\mathrm{d}s + 2\Omega_3 u\Big|_z^h - 2\dot\Omega_1(h-z) \\ &\quad +2\Omega_1 V h_y + 2\Omega_1\int_z^h v_y\,\mathrm{d}s - 2\Omega_2 U h_y - 2\Omega_2\int_z^h u_y\,\mathrm{d}s \\ &\quad -(\Omega_1^2+\Omega_2^2)(h+d_3)h_y - \beta_y(h-z) - \beta h_y - \sigma\partial_y \mathsf{div}(\boldsymbol{\kappa})\,.\end{aligned}$$

or

$$\begin{aligned}\frac{Dv}{Dt} + \frac{1}{\rho}\frac{\partial p}{\partial y} &= \tfrac{Dv}{Dt}\Big|^h + \tfrac{Dw}{Dt}\Big|^h h_y - 2\Omega_1 W + 2\Omega_3 U - 2\dot\Omega_1(h-z) \\ &\quad +2\Omega_1 V h_y - 2\Omega_2 U h_y + 2\Omega_1 w - 2\Omega_3 u \\ &\quad -(\Omega_1^2+\Omega_2^2)(h+d_3)h_y - \beta_y(h-z) - \beta h_y - \sigma\partial_y \mathsf{div}(\boldsymbol{\kappa})\,.\end{aligned} \tag{A-2}$$

which is equation (3.4) in §3.

A.3. *The y−momentum equation*

The $y-$component of the momentum equations (2.5) is

$$\begin{aligned}\frac{Du}{Dt} + \frac{1}{\rho}\frac{\partial p}{\partial x} &= +2(\Omega_1 w - \Omega_3 u) + \dot\Omega_1(z+d_3) - \dot\Omega_3(x+d_1) \\ &\quad -\Omega_2\,\boldsymbol{\Omega}\cdot(\mathbf{x}+\mathbf{d}) + (y+d_2)\|\boldsymbol{\Omega}\|^2 - \mathbf{Q}\mathbf{e}_2\cdot\ddot{\mathbf{q}} - g\mathbf{Q}\mathbf{e}_2\cdot\mathbf{e}_3\,.\end{aligned} \tag{A-3}$$

Now equate (3.4) and (A-3)

$$\begin{aligned}\frac{Dv}{Dt} + \frac{1}{\rho}\frac{\partial p}{\partial y} &= \tfrac{Dv}{Dt}\Big|^h + \tfrac{Dw}{Dt}\Big|^h h_y - 2\Omega_1 W + 2\Omega_3 U - 2\dot\Omega_1(h-z) \\ &\quad +2\Omega_1 V h_y - 2\Omega_2 U h_y + 2\Omega_1 w - 2\Omega_3 u \\ &\quad -(\Omega_1^2+\Omega_2^2)(h+d_3)h_y - \beta_y(h-z) - \beta h_y - \sigma\partial_y \mathsf{div}(\boldsymbol{\kappa}) \\ &\quad -2(\Omega_1 w - \Omega_3 u) - \dot\Omega_1(z+d_3) + \dot\Omega_3(x+d_1) \\ &\quad +\Omega_2\,\boldsymbol{\Omega}\cdot(\mathbf{x}+\mathbf{d}) - (y+d_2)\|\boldsymbol{\Omega}\|^2 + \mathbf{Q}\mathbf{e}_2\cdot\ddot{\mathbf{q}} + g\mathbf{Q}\mathbf{e}_2\cdot\mathbf{e}_3\end{aligned}$$

which after simplification and substitution for β_y becomes

$$\begin{aligned}&\tfrac{Dv}{Dt}\Big|^h + \tfrac{Dw}{Dt}\Big|^h h_y - 2\Omega_1 W + 2\Omega_3 U - \dot\Omega_1(h+d_3) \\ &+2\Omega_1 V h_y - 2\Omega_2 U h_y + \dot\Omega_3(x+d_1) \\ &-(\Omega_1^2+\Omega_2^2)(h+d_3)h_y + \Omega_2\Omega_3(h+d_3) - \beta h_y - \sigma\partial_y \mathsf{div}(\boldsymbol{\kappa}) \\ &+\Omega_2\Omega_1(x+d_1) - (\Omega_1^2+\Omega_3^2)(y+d_2) \\ &+\mathbf{Q}\mathbf{e}_2\cdot\ddot{\mathbf{q}} + g\mathbf{Q}\mathbf{e}_2\cdot\mathbf{e}_3 = 0\end{aligned}$$

Replace W using the kinematic condition

$$W = h_t + Uh_x + Vh_y\,,$$

giving

$$\begin{aligned}
&\left.\frac{Dv}{Dt}\right|^h + \left.\frac{Dw}{Dt}\right|^h h_y - 2\Omega_1(h_t + Uh_x + Vh_y) + 2\Omega_3 U - \dot{\Omega}_1(h + d_3) \\
&+2\Omega_1 V h_y - 2\Omega_2 U h_y + \dot{\Omega}_3(x + d_1) \\
&-(\Omega_1^2 + \Omega_2^2)(h + d_3)h_y + \Omega_2\Omega_3(h + d_3) - \beta h_y - \sigma\partial_y \mathsf{div}(\boldsymbol{\kappa}) \\
&+\Omega_2\Omega_1(x + d_1) - (\Omega_1^2 + \Omega_3^2)(y + d_2) \\
&+\mathbf{Q}\mathbf{e}_2 \cdot \ddot{\mathbf{q}} + g\mathbf{Q}\mathbf{e}_2 \cdot \mathbf{e}_3 = 0
\end{aligned}$$

Now use the fact that

$$V_t + UV_x + VV_y = \left.\frac{Dv}{Dt}\right|^h .$$

Then the surface $y-$momentum equation is reduced to the expression given in (4.7).

†

REFERENCES

Abbott, M. B. 1979 *Computational Hydraulics: Elements of the Theory of Free-Surface Flows*. London: Pitman Publishers.

Adee, B. H. & Caglayan, I. 1982 The effects of free water on deck on the motions and stability of vessels. In *Proc. Second Inter. Conf. Stab. Ships and Ocean Vehicles*, *Tokyo*, vol. 218, pp. 413–426. Springer.

Alemi Ardakani, H. & Bridges, T. J. 2009*a* Coupled roll motion of a liquid-tank system with shallow water. *(in preparation)* .

Alemi Ardakani, H. & Bridges, T. J. 2009*b* Dynamic coupling between shallow water sloshing and horizontal vehicle motion. *Preprint* .

Alemi Ardakani, H. & Bridges, T. J. 2009*c* Review of the 3-2-1 Euler angles: a yaw-pitch-roll sequence. *Tech. Rep.*. Department of Mathematics, University of Surrey.

Alemi Ardakani, H. & Bridges, T. J. 2009*d* Review of the Dillingham, Falzarano & Pantazopoulos three-dimensional shallow-water equations. *Tech. Rep.*. Department of Mathematics, University of Surrey.

Alemi Ardakani, H. & Bridges, T. J. 2009*e* Review of the Huang-Hsiung three-dimensional shallow-water equations. *Tech. Rep.*. Department of Mathematics, University of Surrey.

Alemi Ardakani, H. & Bridges, T. J. 2009*f* Shallow water sloshing in rotating vessels: details of the numerical algorithm. *Tech. Rep.*. Department of Mathematics, University of Surrey.

Alemi Ardakani, H. & Bridges, T. J. 2009*g* Shallow-water sloshing in rotating vessels. Part 1: Two-dimensional flow field. *Preprint* .

Barnes, R. T. H., Hide, R., White, A. A. & Wilson, C. A. 1983 Atmospheric angular momentum fluctuations, length-of-day changes and polar motion. *Proc. Royal Soc. London A* **387**, 31–73.

Billingham, J. 2002 Nonlinear sloshing in zero gravity. *J. Fluid Mech.* **464**, 365–391.

Bridges, T. J. 1987 Secondary bifurcation and change of type for three-dimensional standing waves in finite depth. *J. Fluid Mech.* **179**, 137–153.

Bridges, T. J. 2009 Wave breaking and the surface velocity field for three-dimensional water waves. *Nonlinearity* **22**, 947–953.

Buchner, B. 2002 Green water on ship-type offshore structures. PhD thesis, Technical University of Delft.

Caglayan, I. & Storch, R. L. 1982 Stability of fishing vessels with water on deck: a review. *J. Ship Research* **26**, 106–116.

Cariou, A. & Casella, G. 1999 Liquid sloshing in ship tanks: a comparitive study of numerical simulation. *Marine Structures* **12**, 183–198.

Chen, Y. G., Djidjeli, K. & Price, W. G. 2009 Numerical simulation of liquid sloshing phenomena in partially filled containers. *Computers & Fluids* **38**, 830–842.

Chen, Y.-H., Hwang, W.-S. & Ko, C.-H. 2000 Numerical simulation of the three-dimensional sloshing problem by boundary element method. *J. Chinese Inst. Engin.* **23**, 321–330.

Dillingham, J. 1981 Motion studies of a vessel with water on deck. *Marine Technology* **18**, 38–50.

Dillingham, J. T. & Falzarano, J. M. 1986 Three-dimensional numerical simulation of green water on deck. In *3rd Inter. Conf. Stability of Ships and Ocean Vehicles*. Gdansk, Poland.

† Technical reports are available at the website `http://personal.maths.surrey.ac.uk/st/T.Bridges/SLOSH/`

Disimile, P. J., Pyles, J. M. & Toy, N. 2009 Hydraulic jump formation in water sloshing within an oscillating tank. *J. Aircraft* **46**, 549–556.

Evans, D. J. 1977 On the representation of orientation space. *Molecular Physics* **34**, 317–325.

Faltinsen, O. M., Rognebakke, O. F. & Timokha, A. N. 2003 Resonant three-dimensional nonlinear sloshing in a square basin. *J. Fluid Mech.* **487**, 1–42.

Faltinsen, O. M., Rognebakke, O. F. & Timokha, A. N. 2006*a* Resonant three-dimensional nonlinear sloshing in a square-base basin. part 3. base ratio perturbations. *J. Fluid Mech.* **551**, 359–397.

Faltinsen, O. M., Rognebakke, O. F. & Timokha, A. N. 2006*b* Transient and steady-state amplitudes of resonant three-dimensional sloshing in a square base tank with finite fluid depth. *Physics of Fluids* **18**, 012103.

Faltinsen, O. M. & Timokha, A. N. 2003 An adaptive multimodal approach to nonlinear sloshing in a rectangular tank. *J. Fluid Mech.* **432**, 167–200.

Falzarano, J. M., Laranjinha, M. & Guedes Soares, C. 2002 Analysis of the dynamical behaviour of an offshore supply vessel with water on deck. In *Proc. 21st Inter. Conf. Offshore Mechanics and Artic Eng.*, *Paper No. OMAE2002-OFT28177*, vol. 7. ASME.

Gerrits, J. 2001 Dynamics of liquid-filled spacecraft. PhD thesis, University of Groningen, Netherlands.

Hanson, A. J. 2006 *Visualizing Quaternions*. Amsterdam: Morgan-Kaufmann/Elsevier.

Huang, Z. 1995 Nonlinear shallow water flow on deck and its effect on ship motion. PhD thesis, Technical University of Nova Scotia, Halifax, Canada.

Huang, Z. J. & Hsiung, C. C. 1996 Nonlinear shallow water on deck. *J. Ship Research* **40**, 303–315.

Huang, Z. J. & Hsiung, C. C. 1997 Nonlinear shallow-water flow on deck coupled with ship motion. In *Twenty-First Symposium on Naval Hydrodynamics*, pp. 220–234. National Academies Press.

Ibrahim, R. A. 2005 *Liquid Sloshing Dynamics*. Cambridge: Cambridge University Press.

Kidambi, R. & Shankar, P. N. 2004 The effects of the contact angle on sloshing in containers. *Proc. Royal Soc. London A* **460**, 2251–2267.

Kim, Y. 2001 Numerical simulation of sloshing flows with impact load. *Applied Ocean Research* **23**, 53–62.

Kleefsman, K. M. T., Erwin Loots, G., Veldman, A. E. P., Buchner, B., Bunnik, T. & Falkenberg, E. 2005 The numerical simulation of green water loading including vessel motions and the incoming field. In *Proc. 24th Inter. Cof. on Offshore Mechanics and Artic Engineering*, , vol. OMAE2005-67448. OMAE'05.

Kobine, J. J. 2008 Nonlinear resonant characteristics of shallow fluid layers. *Phil. Trans. Royal Soc. London A* **366**, 1131–1346.

La Rocca, M., Mele, P. & Armenio, V. 1997 Variational approach to the problem of sloshing in a moving container. *J. Theor. Appl. Fluid Mech.* **1**, 280–bbb.

La Rocca, M., Sciortino, G. & Boniforti, M. A. 2000 A fully nonlinear model for sloshing in a rotating container. *Fluid Dynamics Res.* **27**, 23–52.

Lee, S. J., Kim, M. H., Lee, D. H., Kim, J. W. & Kim, Y. H. 2007 The effects of lng-tank sloshing on the global motions of lng carriers. *Ocean Engineering* **34**, 10–20.

Lee, S. K., Surendran, S. & Lee, G. 2005 Roll performance of a small fishing vessel with live fish tank. *Ocean Engineering* **32**, 1873–1885.

Leendertse, J. 1967 Aspects of a computational model for long-period water wave propagation. *Tech. Rep.* RM-5294-PR. Rand Corporation.

Leimkuhler, B. & Reich, S. 2004 *Simulating Hamiltonian Dynamics*. Cambridge: Cambridge University Press.

Leubner, C. 1981 Correcting a widespread error concerning the angular velocity of a rotating rigid body. *Amer. J. Phys.* **49**, 232–234.

Liu, D. & Lin, P. 2008 A numerical study of three-dimensional liquid sloshing in tanks. *J. Comp. Phys.* **227**, 3921–3939.

Miles, J. & Henderson, D. 1990 Parametrically forced surface waves. *Ann. Rev. Fluid Mech.* **22**, 143–165.

Murray, R. M., Lin, Z. X. & Sastry, S. S. 1994 *A Mathematical Introduction to Robotic Manipulation*. Boca Raton, Florida: CRC Press.

O'Reilly, O. M. 2008 *Intermediate Dynamics for Engineers: a Unified Treatment of Newton-Euler and Lagrangian Mechanics*. Cambridge: Cambridge University Press.

Pantazopoulos, M. S. 1987 Numerical solution of the general shallow water sloshing problem. PhD thesis, University of Washington, Seattle.

Pantazopoulos, M. S. 1988 Three-dimensional sloshing of water on decks. *Marine Technology* **25**, 253–261.

Pantazopoulos, M. S. & Adee, B. H. 1987 Three-dimensional shallow water waves in an oscillating tank. *Proc. Amer. Soc. Civil. Eng.* pp. 399–412.

Penney, W. G. & Price, A. T. 1952 Part II. Finite periodic stationary gravity waves in a perfect fluid. *Phil. Trans. Royal Soc. London A* **244**, 254–284.

Peregrine, D. H. 1998 Surf-zone currents. *Theor. Compl. Fluid Dynamics* **10**, 295–309.

Peregrine, D. H. 1999 Large-scale vorticity generation by breakers in shallow and deep water. *Eur. J. Mech. B/Fluids* **18**, 403–408.

Pomeau, Y., Berre, M. Le, Guyenne, P. & Grilli, S. 2008*a* Wave breaking and generic singularities of nonlinear hyperbolic equations. *Nonlinearity* **21**, T61–T79.

Pomeau, Y., Jamin, T., Le Bars, M., Le Gal, P. & Audoly, B. 2008*b* Law of spreading of the crest of a breaking wave. *Proc. Royal Soc. London A* **464**, 1851–1866.

Rapaport, D. C. 1985 Molecular dynamics simulations using quaternions. *J. Comp. Phys.* **60**, 306–314.

Romero, I. 2008 Formulation and performance of variational integrators for rotating bodies. *Comput. Mech.* **42**, 825–836.

Ruponen, P., Matusiak, J., Luukkonen, J. & Ilus, M. 2009 Experimental study on the behavior of a swimming pool onboard a large passenger ship. *Marine Technology* **46**, 27–33.

Taylor, G. I. 1953 An experimental study of standing waves. *Proc. Royal Soc. London A* **218**, 44–59.

Titterton, D. H. & Weston, J. L. 2004 *Strapdown Inertial Navigation Technology*, 2nd edn. UK: Institute of Electrical Engineers.

Veldman, A. E. P., Gerrits, J., Luppes, R., Helder, J. A. & Vreeburg, J. P. B. 2007 The numerical simulation of liquid sloshing on board spacecraft. *J. Comp. Physics* **224**, 82–99.

aus der Wiesche, S. 2003 Computational slosh dynamics: theory and industrial application. *Comp. Mech.* **30**, 374–387.

Wu, C.-H. & Chen, B.-F. 2009 Sloshing waves and resonance modes of fluid in a 3D tank by a time-independent finite difference method. *Ocean Eng.* **36**, 500–510.

Wu, G. S., Ma, Q. W. & Eatock Taylor, R. 1998 Numerical simulation of sloshing waves in a 3D tank based on a finite element method. *Appl. Ocean Res.* **20**, 337–355.

Zhou, Z., Kat, J. O. De & Buchner, B. 1999 A nonlinear 3D approach to simulate green water dynamics on deck. In *Proc. 7th Inter. Conf. Numer. Ship Hydro.* (ed. J. Piquet), *Nantes*, vol. 7. DTIC.